TECHNICAL MEMORANDUM

576

Exploitation of satellite data in the surface analysis

M. Drusch, K. Scipal, P. de Rosnay,
G. Balsamo, E. Andersson,
P. Bougeault, P. Viterbo

Research Department

Presented to the 37th Session of the
Scientific Advisory Committee (SAC)

October 2008

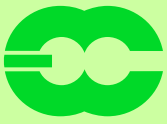

European Centre for Medium-Range Weather Forecasts
Europäisches Zentrum für mittelfristige Wettervorhersage
Centre européen pour les prévisions météorologiques à moyen terme

Series: ECMWF Technical Memoranda

A full list of ECMWF Publications can be found on our web site under:
http://www.ecmwf.int/publications/

Contact: library@ecmwf.int

European Centre for Medium-Range Weather Forecasts
Shinfield Park, Reading, RG2 9AX, England

Abstract

This paper presents the ECMWF surface analysis system and its recent developments. A short description of the ECMWF land surface model HTESSEL (Hydrology Tiled ECMWF Scheme for Surface Exchanges over Land) is provided. In contrast to the previous version (TESSEL), HTESSEL accounts for geographically varying soil texture and variable infiltration capacity. This improves the simulated soil moisture range and soil moisture dynamics. Model validation is illustrated by using field experiments data set in two contrasted areas. Soil moisture is a key component of the surface-atmosphere water and energy fluxes representation. Its parameterisation in the land surface model influences the surface analysis and controls the strength of the feedbacks between the surface analysis and the forecast model.

The ECMWF surface analysis system is presented. Some deficiencies with the current Optimal Interpolation (OI) soil-moisture scheme are demonstrated, which have motivated the development of a new surface analysis scheme. The new scheme is a point-wise Extended-Kalman Filter (EKF) for the global land surface, built on the concepts developed in the European Land Data Assimilation System (ELDAS) project. The EKF surface analysis will facilitate combined use of satellite, in situ and proxy observations. Initial results using the same proxy observations as in the OI (2m air temperature and relative humidity) are shown.

Satellite data from active or passive microwave sensors are highly suitable for soil moisture remote sensing. The EKF surface analysis opens the possibility to use these different actual and future data types for the soil moisture analysis. To this end appropriate observation operators have been developed and evaluated. They are presented in this paper.

The soil moisture information in the C-band Advanced SCATerometer (ASCAT) and in European Remote Sensing (ERS) scatterometer data (active microwave) has been investigated. ASCAT product is shown to contain valuable information about soil moisture specifically in tropical, dry and temperate climates. An observation operator that matches the European Organisation for the Exploitation of Meteorological Satellites (EUMETSAT) scatterometer soil-moisture product with the model's soil moisture has been developed. A demonstration experiment shows the value of this approach and first results of ASCAT soil moisture assimilation using the EKF surface analysis are presented.

The future Soil Moisture and Ocean Salinity (SMOS, to be launch in spring 2009) L-band radiances (passive microwave) are to be assimilated directly in the EKF surface analysis system, without first being converted to soil moisture. This approach relies on the availability of an accurate forward model (observation operator) capable of simulating the observations from the quantities represented by the forecast model, i.e. a microwave surface emissivity model. The Community Microwave Emission Model (CMEM) model has been developed at ECMWF for this purpose and it is presented in this paper. It incorporates a large number of parameterisation options. One option reproduces exactly the results of the forward model adopted by ESA's development team for the SMOS retrieval algorithm. Calibration and sensitivity studies have been performed at different spatial scales with Skylab data, AMSR-E (Advanced Microwave Scanning Radiometer on Earth Observing System) data and SMOSREX (Soil Monitoring Of the Soil Reservoir EXperiment) field data for different microwave emission parameterisations considered in CMEM. In particular a combined inter-comparison between Land Surface Models (LSMs) and surface emissivity models has been conducted and validated against AMSR-E C-band measurements. These studies allow quantitative assessment of the sensitivity of the simulated surface emission to the coupled LSM-microwave emission model components. They point out the optimal microwave modelling configuration that best reproduces the top of atmosphere brightness temperature at different frequencies and at different spatial scales.

The new EKF surface analysis system opens a range of further development possibilities, exploiting new satellite surface data and products for the assimilation of soil moisture. It is implemented in the research branch of the ECMWF Integrated Forecast System (IFS) and it is currently under evaluation and validation. Short term objectives for 2009 focus on the operational implementation of the EKF surface analysis. This requires solving the computing time cost issue by revising the structure of the surface analysis within the ECMWF forecast system. Long term objectives encompass an extention of the EKF surface analysis to account for additional variables such as snow mass and vegetation parameters. This work relies on parallel developments in the land surface model concerning the vegetation dynamics, snow and ice.

1 Introduction

Within ECMWF's Integrated Forecast System (IFS), the surface analyses provide the initial conditions at the forecast model's lower boundary. During the integration of the forecast model, the surface is fully coupled to the atmosphere. The surface processes and the related variables (land surface energy and water fluxes, soil moisture and soil temperature, snow cover and snow mass, water content intercepted by vegetation) interact with the atmospheric variables such as wind, precipitation, temperature and radiation. In contrast the surface analysis is independent from the atmospheric model and independent from the 4D-Var atmospheric analysis. There is a feedback between model and analysis in that the model-predicted surface fields provide the background (first guess) for the following surface analysis and in turn the analysis provides the initial conditions to the forecast model.

The individual components of the surface analysis -snow, Sea Surface Temperature (SST), sea-ice cover (CI), soil moisture and soil temperature- are also performed independent from each other, apart from empirical consistency checks (e.g. the sea ice analysis uses the analysed SST for quality control). The complexity of the individual surface analyses differs but is far less than that of the atmospheric 4D-Var, and computationally they are several orders of magnitude less expensive. A schematic view of the current surface analysis systems is given in Figure 1 (left), and it is shown with respect to what we would consider the ideal, comprehensive surface analysis system (right panel). This schematic representation shows a range of parameters (2nd circle) that when taken together represent the state of the land and ocean surfaces and vegetation. Effective analysis of these parameters (3rd circle) depends on various modelling components (1st circle) that describe the interactions between the surface and the atmosphere (centre). We can see that several surface modelling components are missing from the current forecast system, and the range of analysed parameters is incomplete. Some variables are analysed without two-way interaction with the Integrated Forecast System (IFS) model atmosphere, or rely on externally derived products or climatology. The long-term goal is to implement the missing elements in order of priority. Current work focuses on soil moisture analysis and on the vegetation and the carbon cycle supported by the GEOLAND and GEMS projects.

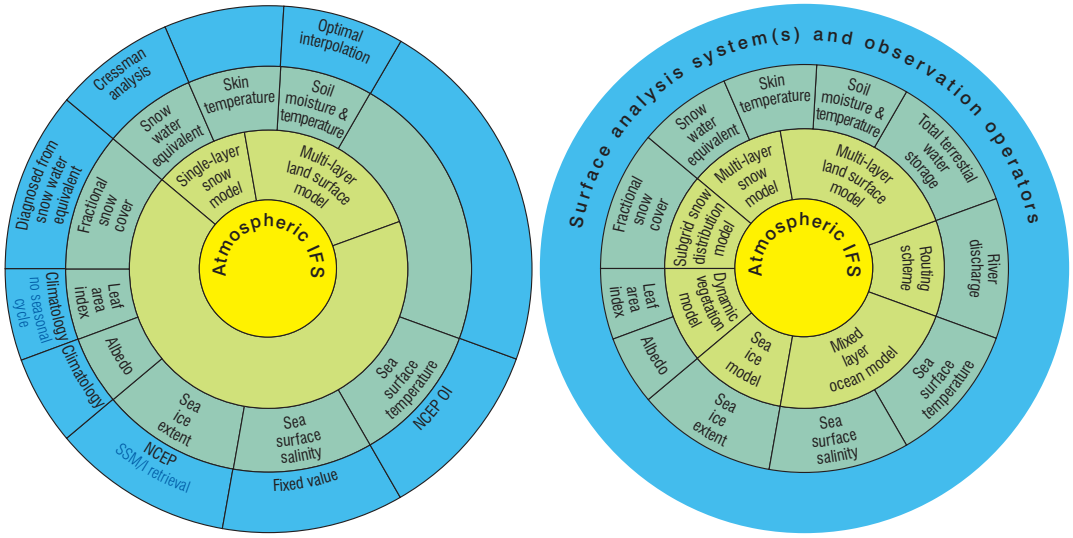

Figure 1: Schematic view of the current (left) and extended (right) surface analysis systems used for deterministic Numerical Weather Prediction.

1.1 Sea ice and sea surface temperature

The previous operational (IFS cycle 33R1, in operations from 06 June to 29 September 2008) CI and SST analyses relied on global data products provided by NCEP's (National Center for Environmental Prediction) Marine Modeling and Analyses Branch. The daily SST fields were based on satellite observations from the thermal infra red, buoy measurements and ship observations, which are integrated through an Optimal Interpolation scheme. The CI fields have been derived from SSM/I (Special Sensor Microwave Imager) data following Grumbine (1996). Both data sets are received on a 0.5^o regular grid and re-sampled to the reduced Gaussian grid using a bi-linear interpolation scheme. Sea-surface salinity is assimilated by the ocean model used for seasonal forecasting, but is currently not provided to the atmospheric model. The SST and CI analyses have been modified and implemented in the current operational IFS cycle (33R2, in operation since 30 September 2008). The high-resolution Operational Sea Surface Temperature and Sea Ice Analysis (OSTIA) data set produced by the UK Met Office (Stark et al., 2007), and the accompanying CI produced by EUMETSAT's Ocean and Sea-Ice Satellite Application Facility (OSI-SAF) are used. The OSTIA SST uses observations from a range of satellite instruments: infrared and microwave imagers and sounders. The OSTIA data has a much better representation of the small-scale eddies and SST gradients than the current NCEP product at 0.5^o. Perhaps more importantly, the microwave remote sensing data enables an all-weather capability to the SST product, particularly beneficial for the persistent stratocumulus oceanic areas. A conserving interpolation scheme is used to aggregate the 0.05^o data to the model's Gaussian grid which preserves the area-averaged temperature (*Holm, ECMWF, personal communication*).

1.2 Snow mass and snow fraction

Snow mass is analysed every six hours through a Cressman spatial interpolation. Apart from in-situ observations satellite-derived snow cover data from NOAA (National Oceanic and Atmospheric Administration)/NESDIS (National Environmental Satellite, Data and Information Service) are used. The implementation of this snow analysis and an evaluation of the snow mass fields can be found in Drusch et al. (2004) and Drusch (2005). Fractional snow cover is diagnosed from snow mass through an empirical relationship.

1.3 Soil moisture

The screen level parameters temperature and relative humidity at 2 m height are technically part of the surface analysis. Both parameters are analysed through an Optimal Interpolation (OI) scheme based on conventional SYNOP observations only. Analysis increments of T_{2m} and RH_{2m} are then used as proxy observations for use in the soil moisture and soil (or snow) temperature OI analyses. Soil moisture is analysed in snow free areas only.

Over the past few years, we have focused on the work to extend the use of satellite-derived surface data and products. The main prospects in this regard are for improvements of the soil-moisture analysis. Here, the exploitation of new technology in both passive and active microwave remote-sensing promises to deliver valuable data on near-surface soil moisture. This work is carried out within the framework of EUMETSAT's Hydrology Satellite Application Facility (H-SAF) supporting the exploitation of ERS and ASCAT soil moisture products, and in preparation for European Space Agency (ESA) Soil Moisture and Ocean Salinity (SMOS) mission. The latter is an Earth Explorer demonstration mission and the first satellite instrument dedicated to soil moisture.

1.4 The motivations for soil-moisture analysis development

Evapotranspiration is one of the most important parameters for the definition of the thermodynamic and moisture content of the lower troposphere over land. For a given amount of radiative energy available at the surface, the partitioning between the latent heat and sensible heat influences the evolution of the screen level parameters, e.g. 2 m temperature and relative humidity, sub-cloud layer entropy and water, boundary layer clouds, height of cloud base and consequently precipitation. Evapotranspiration is controlled by soil moisture in dry-down periods when potential evaporation is high. The influence of soil moisture on the atmosphere has been shown on the local scale (Seuffert et al., 2002), the regional scale (Schär et al., 1999), and the continental to global scale (Ferranti and Viterbo, 2006; Koster, R. et al., 2004; Shukla and Mintz, 1982). ECMWF's current work programme on soil moisture is motivated by these findings, and is expected to benefit predictions at all time ranges. The present availability of satellite soil moisture observations providing near-global coverage is another important impetus for this work.

The key parameter for a correct description of the actual evapotranspiration is root zone soil moisture. Even on regional scales only very few measurements of this quantity exist. Consequently, proxy observations and modelled soil moisture fields are used to initialise soil moisture in numerical weather prediction (NWP). Calvet et al. (1998) and Walker et al. (2002) have shown that, if in-situ observations of surface-soil moisture are provided, root-zone soil-moisture can be retrieved. In the past years, a number of studies assessed the potential of remotely-sensed observations for the soil-moisture analysis. These measurements comprise infrared heating rates (van den Hurk et al., 1997), passive microwave brightness temperatures (Reichle et al., 2001; Crow and Wood, 2003), soil moisture derived from passive and active systems (Reichle and Koster, 2005; Pauwels et al., 2002) and combinations of the proxy data (Seuffert et al., 2004). In hydrological models, observed river-discharge measurements have been assimilated as another indirect source of information on root zone soil moisture (Pauwels and Lannoy, 2006). However, for various reasons most of these observations are not operationally available in near-real time and on large spatial scales.

A number of current operational soil moisture analysis systems in NWP are based on analysed or observed screen-level variables, i.e. 2m temperature and relative humidity. At Météo France (Giard and Bazile, 2000), ECMWF (Douville et al., 2000; Mahfouf et al., 2000; Mahfouf, 1991), the Canadian Meteorological Centre (Bélair et al., 2003) and in the High Resolution Limited Area Model (HIRLAM, Rodriguez et al., 2003) Optimal Interpolation algorithms (Rutherford, 1972) are used operationally. This method requires specification of observation and background errors in order to obtain the analysed state. A weakness of these implementations is that the statistics of background error have been derived at a single location, using data from Monte-Carlo experiments with a single-column version of a coupled land-surface - atmosphere model (HAPEX-MOBILHY). In an effort to avoid this dependence on pre-specified background errors, the German Weather Service, developed a 'simplified' Extended Kalman Filter (EKF) (Hess, 2001), which is now operational at DWD (Deutsche Wetter Dienst). Météo-France recently developed an offline EKF soil analysis scheme within the SURFace EXternalized (SURFEX) version of their land surface model (Mahfouf et al., 2008).

This paper presents the ECMWF surface analysis system and its recent developments based on the implementation of an EKF within the IFS. It focuses on soil moisture analysis which is a key variable of the surface-atmosphere interface. But it is envisaged that the new scheme could be extended to other surface variables, and that these will be analysed simultaneously. Section 2 presents the operational Land Surface Model HTESSEL (Hydrology - Tiled ECMWF Scheme for Surface Exchanges over Land) which accounts for a revised representation of the soil hydrology. Section 3.1 describes the operational soil-moisture OI analysis scheme and its shortcomings as evidenced by a set of nudging experiments using satellite data products. The new surface analysis scheme based on the EKF concept is described in Section 3.3. The EKF surface analysis will facilitate combined use of satellite, in situ and proxy observations. In the EKF, the Jacobians of the surface model and

the observation operators describe the link between the observations and the analysed variables. The introduction of satellite observations in the EKF surface analysis thus requires development of accurate observation operators. Prognostic simulation of soil moisture by HTESSEL is used in the EKF surface analysis as an input of the forward modelling approaches which are described in some detail in Sections 4 and 5 for active and passive observations. The preparatory studies on the interpretation and exploitation of ASCAT and SMOS data is presented in these two sections. In the case of SMOS a land surface emissivity model is required to compute the model equivalent of the observed brightness temperature. The final Section (6) provides a summary and outlook.

2 The Land Surface Model

The land surface component of the forecast model is essential to simulate the water fluxes to the atmosphere and the river runoff (van den Hurk et al., 2005). The energy repartition at the surface is largely determined by the soil moisture, and this has a direct influence on the air temperature and humidity in the boundary layer. The TESSEL scheme (Tiled ECMWF Scheme for Surface Exchanges over Land, van den Hurk et al., 2000) was operational in the IFS from the cycles 22R3 to 32R2 (from to June 2000 to November 2007) and it has been used in ECMWF's re-analysis projects.

In TESSEL up to 6 tiles are considered over land (bare ground, low and high vegetation, intercepted water, shaded and exposed snow) and 2 over water (open and frozen water), each with its separate energy and water balances. The vertical discretisation considers a four-layer soil that can be covered by a single layer of snow. The depths of the soil layers are in an approximate geometric relation, as suggested in Deardorff (1978). Warrilow et al. (1986) have shown that a four-layer soil discretisation provides a reasonable compromise between computational cost and the ability to represent all timescales between one day and a year. The soil energy budget follows a Fourier diffusion law, modified to take into account soil water freezing and melting according to Viterbo et al. (1999). The soil energy budget equation is solved with a net ground heat-flux as the top boundary condition and zero flux as the lower boundary condition.

The interception layer accumulates precipitation until the layer is saturated. Any excess precipitation (throughfall) is partitioned between surface runoff and infiltration into the soil. Subsurface water fluxes are determined by Darcy's law, used in a soil water equation solved with a four-layer discretisation shared with the heat budget equation. The top boundary condition is infiltration plus surface evaporation. Free drainage is assumed at the bottom. Each layer has an additional sink of water in the form of root extraction in vegetated areas. In each grid box two vegetation types are present: a high and a low vegetation type. An external climate database is used to obtain the vegetation characteristics, based on the Global Land Cover Characteristics (GLCC) data (Loveland et al., 2000, `http://edcdaac.usgs.gov/glcc/glcc.html`). The nominal resolution is 1 km. The data provides for each pixel a biome classification based on the Biosphere-Atmosphere Transfer Scheme (BATS) model (Dickinson et al., 1993), and four parameters have been derived for each grid box: dominant vegetation type, T_H and T_L, and the area fraction, A_H and A_L, for each of the high- and low-vegetation components, respectively.

The vertical movement of water in the unsaturated zone of the soil matrix obeys the following Richards (1931) equation for the volumetric water content θ and account for the root extraction by considering a sink term Viterbo and Beljaars (1995). TESSEL adopts the Clapp and Hornberger (1978) formulation of hydraulic conductivity and diffusivity as a function of soil-water content; see also Mahrt and Pan (1984) for a comparison of several formulations and Cosby et al. (1984) for further analysis. Cosby et al. (1984) tabulate best estimates of the soil hydraulic parameters, for the 11 soil classes of the US Department of Agriculture (USDA) soil classification, based on measurements over large samples. Viterbo and Beljaars (1995) adopted an averaging

procedure to calculate a globally uniform medium-textured (loamy) set of soil parameters used in TESSEL, compatible with the Clapp and Hornberger expression for the matric potential and following Hillel (1982) and Jacquemin and Noilhan (1990).

The water transport is also represented in partially frozen soils. It uses the effective hydraulic conductivity and diffusivity as weighted averages of the values for total liquid soil water and a very small value for frozen soil water as detailed in Viterbo et al. (1999). The soil properties, as defined above, also imply a maximum infiltration rate at the surface defined by the maximum downward diffusion from a saturated surface. In general when the water flux at the surface exceeds the maximum infiltration rate, the excess water is put into surface runoff. The general formulation of surface runoff can be written as $R = T + M - I_{max}$ where I is the infiltration rate. Different runoff schemes differ in the formulation of the infiltration. The maximum infiltration or Hortonian runoff, represent the runoff process at local scales. In TESSEL the maximum infiltration rate I_{max} is calculated as a function of the hydraulic coefficient and the relative soil moisture in the surface layer (0-7cm) (Viterbo et al., 1999).

2.1 Improved hydrology: HTESSEL

A revised hydrology (Balsamo et al., 2008) was introduced in the IFS cycle 32R3 (operational since 7 November 2007) was developed in response to known weaknesses of the TESSEL hydrology. The new HTESSEL scheme includes the following revisions to the soil hydrology: (i) a spatially varying soil type replacing the single loamy soil, (ii) the Van Genuchten (VG) formulation of soil hydraulic properties replacing the Clapp and Hornberger (CH) scheme, and (iii) the surface runoff according to a variable infiltration capacity based on soil type and local topography.

In HTESSEL two adjacent model grid-points with equal surface conditions and equal precipitation may have different surface runoff, depending on the terrain complexity. The soil water drainage depends on the soil texture class. Whenever rain or snow melt occurs, a fraction of the water is removed as surface runoff. The runoff to precipitation ratio scales with the standard deviation of orography, and therefore depends on the complexity represented in the grid box, as well as on soil texture and soil water content. In particular, the surface component of the runoff increases with terrain complexity, soil texture (moving from coarse to fine textures), and soil water content (from dry to wet soil).

2.2 Validation of HTESSEL

The validation focuses on well instrumented sites where various types of observations are available and where the soil type is likely to play a significant role in the surface model behaviour. Long time series (one year or more) of hourly observations of low level wind, temperature and moisture, together with precipitation and downward radiation are used as input to the land surface model. Two different sites are considered for offline simulations comparing TESSEL and HTESSEL, namely SEBEX (Sahelian Energy Balance EXperiment) in the Sahel and BERMS (Boreal Ecosystem Research and Monitoring Sites) in Canada. For each site, vegetation parameters (fraction and types) were assigned to those of the operational high resolution forecast model (at about 25km globally) adopting the nearest gridbox. The sites correspond to different soil textures and to extremely contrasting climatic conditions.

2.2.1 SEBEX Sahel

The Sahelian Energy Balance EXperiment (Wallace et al., 1991) is characterised by a desert climate with fallow savannah vegetation and sandy soil. Volumetric soil moisture reaches extremely low values in the dry season. This dynamical range is typical for sandy soil and can not be represented by the medium texture used in TESSEL, resulting in a much wetter range. Observations of both soil moisture and evaporation are available for verification, as previously considered in van den Hurk et al. (2000). Figure 2 shows the time series of soil moisture. It is clear that the soil moisture range is much better represented by the HTESSEL scheme. This results also in a slightly better match for evaporation during the dry season. TESSEL retains too much water for this desert savannah site.

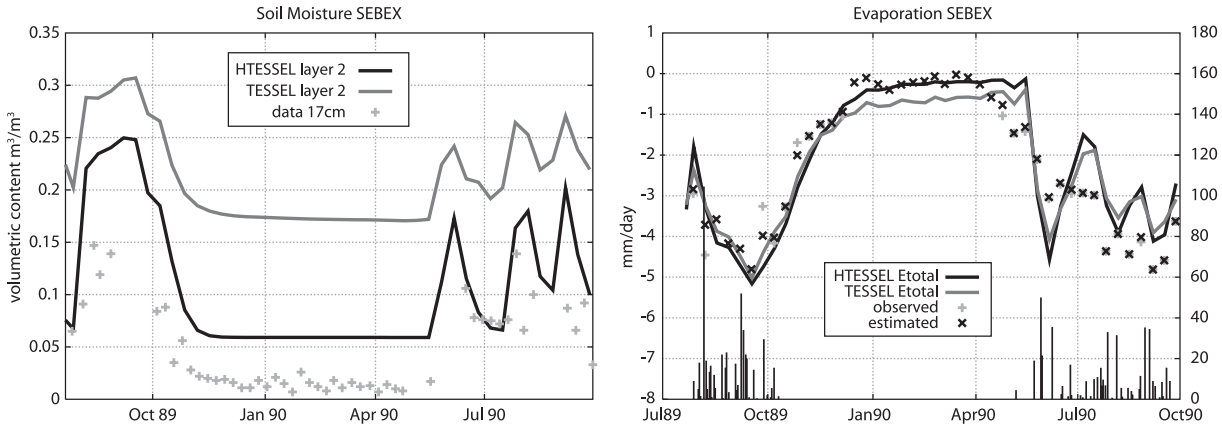

Figure 2: TESSEL (grey line) and HTESSEL (black line) compared to observations (grey +) and local estimates (black x): Left: volumetric soil moisture; and right: evaporation (negative for upward fluxes). The bars indicate daily precipitation in mm (right hand scale).

2.2.2 BERMS Boreal Forest

The BERMS Old Aspen site located in Canadian Boreal forest (central Saskatchewan) has a high soil water retention. The data have been used for the validation of fluxes from ERA-40 in Betts et al. (2006). BERMS data represents one of the longest comprehensive time-series available for land surface model verification. It has marked interannual variability, allowing the evaluation of multiple time scales. Compared to the SEBEX site, TESSEL soil texture (medium) properties are closer to HTESSEL (medium-fine, according to the Food and Agriculture Organization -FAO- data). Still, both the absolute values and the interannual variability of soil moisture are better captured by the HTESSEL as shown in Figure 3. This is explained by a more appropriate soil texture and by the increased memory in the van Genuchten hydrology scheme.

2.3 Land surface model summary

A revised soil hydrology scheme HTESSEL has been introduced in the ECMWF operational model, to address shortcomings of the land surface scheme. A global uniform soil texture and consequently a unique soil moisture range have been addressed by the introduction of a global soil texture map. The lack of surface runoff has been addressed by considering sub-grid scale effects. New infiltration and runoff schemes have been adopted with a dependency on the local soil texture and standard deviation of orography. A set of experiments in stand-alone mode has shown an improved prediction of soil moisture at field sites. From the two contrasting sites presented

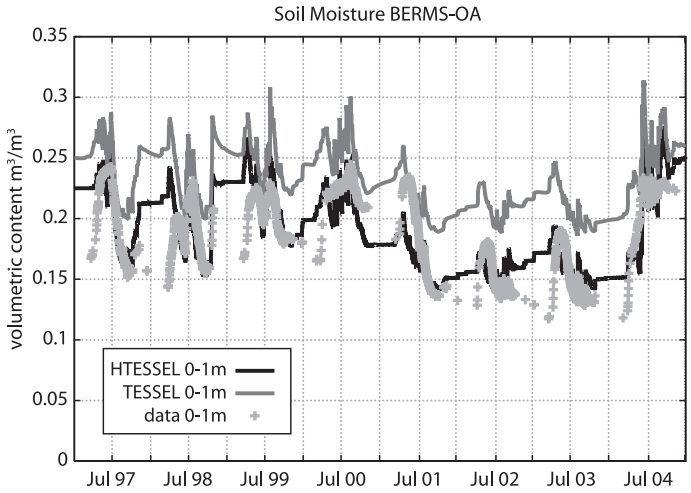

Figure 3: Volumetric soil moisture in TESSEL (grey line) and HTESSEL (black line) compared to observations (light grey +) for BERMS Old Aspen Boreal forest Canada.

here, it is clear that a substantial part of the spatial variability in soil moisture is related to soil properties. The revised soil hydrology represents a step forward for the assimilation of land surface microwave radiances since the improvement in soil moisture reflects onto the land microwave signature, leading to substantially reduced biases as we will see in the following sections. Another land surface model aspect that is important for soil moisture data assimilation, and might need further attention, is the relation between soil moisture and evaporation. The latter is important for the atmospheric forecast and in order to benefit from soil moisture observation, this relation has to be realistic.

3 Soil Moisture Analysis

Soil moisture analyses are produced using an Optimal Interpolation (OI) method as described in Mahfouf et al. (2000). They are scheduled to run immediately after the two main 4D-Var atmospheric analyses. To match the 12-hour 4D-Var period from 09 to 21 UTC (and from 21 to 09 UTC), the soil moisture analysis are performed at 12 and 18 UTC (and at 00 and 06 UTC). These analyses are performed with a delayed cut-off time which allows to account for the maximum possible number of observations. Resulting analysed fields are then used as initial conditions of a short-term forecast which is performed from 18 to 09 UTC (and 06 to 21 UTC). The short-term forecast provides the background (or first guess) fields for both the atmosphere and the surface analysis of the next 4D-Var window. The short-term forecast is also used to initiate a 6-hour 4D-Var analysis performed in the continuity of the 12-hour delayed cut-off analysis, from 21 to 03 UTC (and from 09 to 15 UTC). It is followed by an additional surface analysis at 00 UTC (and 12 UTC). These are the early delivery analyses (4D-Var and surface analysis) which provide initial conditions for the 10-day forecast at 00 UTC (and 12 UTC). For a detailed description of the forecast system we refer to Haseler (2004) and http://www.ecmwf.int/research/ifsdocs/.

3.1 The current operational Optimal Interpolation scheme

Independent analyses of 2 m temperature and relative humidity are produced daily at 00, 06, 12, and 18 UTC using 2-d OI spatial interpolation, and they constitute the main inputs to the current soil moisture analysis. Firstly, the model background, i.e. the 6- or 12-hour forecast, is interpolated horizontally to the observation

locations to compute first guess departures at each observation location. Analysis increments of 2 m temperature and relative humidity are computed at each model grid point. The 2 m analysis increments for temperature T and relative humidity RH are then used to analyse the soil water content θ of each soil layer i separately:

$$\Delta\theta_i = \alpha \times (T_a - T_b) + \beta \times (rH_a - rH_b) \quad (1)$$

with subscripts a and b indicating the analysis and background respectively. The soil moisture analysis relies essentially on the coefficients α and β, also known as optimum coefficients, which account for statistics of forecast and observation errors. Details on the empirical functions can be obtained from `http://www.ecmwf.int/research/ifsdocs/` (IFS cycle 31R1, Chapter II,12). Error statistics for the computation of the optimum coefficients are static. They were derived from a set of Monte Carlo experiments as described in Bouttier et al. (1993) and they have been computed following Douville et al. (2000), considering observation and background errors of 2 K and 1.5 K for temperature and 10 % and 5 % for relative humidity, respectively.
The analysis exploits the relationship between soil moisture and near-surface atmosphere established by evaporation processes, therefore the optimal coefficients are reduced in situations with weak radiative forcing and over mountainous areas when correlation becomes weaker. As a final quality check, soil moisture increments are set to 0 if (i) the last 6-hour precipitation computed from the model exceeds 0.6 mm, (ii) the instantaneous wind speed exceeds 10 ms^{-1}, (iii) the air temperature is below freezing, or (iv) modelled snow is present at the surface.

3.2 Performance of the operational soil-moisture analysis

3.2.1 Assessment of analysis increments and forecast impact

The forecast impact of the surface analysis has been assessed in a 61-day experiment in June-July 2002, using the IFS cycle 29R1 (Drusch and Viterbo, 2007), operational from 5 April 2005 to 26 June 2005. Ten day forecasts were performed from 12 UTC base-times. Results from two experiments were compared:

- CTRL - the control experiment using the Optimal Interpolation soil moisture analysis as described above.
- OL - the open loop experiment, in which soil moisture evolves freely.

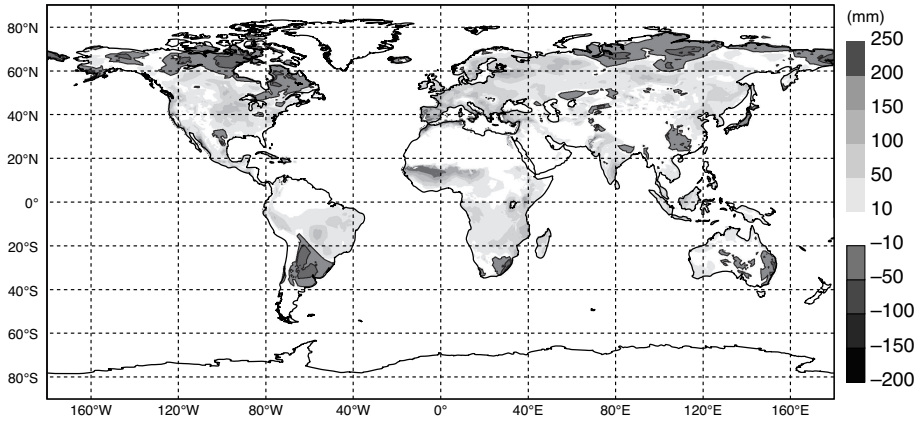

Figure 4: Accumulated root zone (top 1 m soil layer) soil moisture analysis increments (mm) for 2 June to 30 July as obtained from the CTRL OI experiment.

Soil moisture analysis increments (i.e. analysis minus first guess) for the root zone have been computed and accumulated over the period from 2 June to 30 July (Figure 4). In general, the OI analysis scheme adds water to the root zone. Maximum values exceeding 170 mm for the two months period can be found north of the equator in western Africa. Similar values, although on a much smaller spatial scale, are obtained for regions on the Iberian peninsula. The accumulated analysis increments in the central U.S. and central South America can be as high as 105 and 120 mm, respectively. There are only very few areas where the analysis removes water from the soil. Minimum values of -90 mm can be found over parts of Argentina. Average values of analysis increments are an indicator of the quality of a forecast system: persistent analysis corrections are a clear sign of systematic model errors. The values shown in Figure 4 are non-negligible and represent a sizeable part of the terrestrial water budget.

The t-test and the sign-test (van Storch and Zwiers, 1999) have been used to quantify the statistical significance of the differences on forecast performances, in terms of temperature. Table 1 summarises the results for different areas and pressure levels. The results for the Northern Hemisphere indicate that the soil moisture analysis improves the forecast quality significantly for up to 9 days for the lower atmospheric levels. A positive impact on the short-range forecast (up to day 3) can even be found for temperatures at 700 hPa pressure level. In general, these positive impacts on the forecast skill have been obtained for continental areas in Europe, East Asia, and North America.

Area	Height[hPa]	Forecast time [hours]				
		24	72	120	168	216
N. Hemisphere	1000	0.1 / 0.1	0.1 / 0.1	0.1 / 0.5	2.0 / 10.0	- / 1.0
	850	0.1 / 0.1	0.1 / 0.1	0.1 / 5.0	- / -	- / 5.0
	700	- / 5.0	2.0 / 1.0	- / -	- / -	- / 10.0
Europe	1000	0.1 / 0.1	0.1 / 0.1	0.2 / 0.1	- / -	- / -
	850	0.1 / 0.1	0.1 / 0.1	5.0 / 5.0	- / -	- / -
	700	- / -	- / 10.0	- / -	- / -	- / -
East Asia	1000	0.1 / 0.1	0.1 / 0.1	5.0 / 0.1	- / 5.0	0.5 / 0.5
	850	0.1 / 0.1	5.0 / 0.1	2.0 / 5.0	- / -	0.1 / 0.2
	700	2.0 / -	- / -	- / -	- / -	- / 5.0
N. America	1000	0.1 / 0.1	1.0 / 0.1	- / -	- / -	- / -
	850	0.1 / 0.1	0.2 / 0.1	- / -	- / -	- / -
	700	- / 5.0	- / -	- / -	- / -	- / -

Table 1: Significance levels for the t-test (first value) and sign-test (second value, in %). CTRL and OL experiment are compared based on RMS forecast errors of temperatures at 700 hPa pressure level. The numbers represent cases where the CTRL experiment is better than the OL experiment. Dashes indicate cases for which no significant difference has been found.

3.2.2 Comparison against in situ observations

Since the screen-level variables ($T2m$ and $RH2m$) that are assimilated into the current soil moisture analysis are only proxy observations for root-zone soil moisture it is imperative to compare the analysed soil moisture against independent in-situ observations. Generally, it is difficult to compare in-situ observations representing the point scale against a (rather coarse resolution) model grid box value since the spatial variability of soil moisture is high. For the actual study period of June and July 2002, the best suited verification data have been obtained from the Oklahoma Mesonet.

The Oklahoma Mesonet consists of over 110 automated stations. Each site is equipped with a set of instruments located on or near a 10 m tower. For this study, 72 stations reporting soil moisture observations for the data as-

similation experiment period on a regular basis have been selected. The observations comprise air temperature and relative humidity at 1.5 m above the ground, wind speed and direction measured at 10 m height, rainfall, pressure, and incoming solar radiation. In addition, most of the stations observe soil moisture at 0.05, 0.25, 0.6, and 0.75 meters below the ground. The complete description of the network and its instrumentation can be found under http://www.mesonet.org.

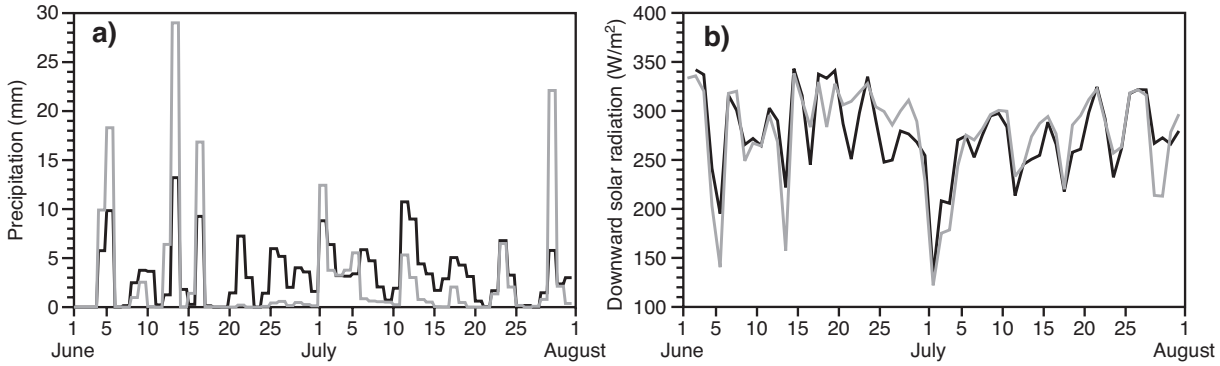

Figure 5: Observed (grey line) and modelled (black line) daily rainfall (a) and downward solar radiation (b) for the Oklahoma area. Total area averages have been computed from the 12-h forecasts starting at 0600 and 1800 UTC base times for the CTRL OI experiment.

It is well known that the accuracy of modelled soil moisture strongly depends on the quality of the meteorological atmospheric forcing data, particularly precipitation and incoming solar radiation. Both quantities have been observed at the OK Mesonet sites. In Figure 5 we compare the observed and modelled precipitation. We see that the model tends to underestimate large amounts of rainfall for the first half of June and the end of July, which is a known model bias. Significant differences also occurred in the second half of June and the middle of July, when the model precipitation exceeds the observed amount. The total amount of rainfall in June is 87.3 mm on 19 rainy days in the model and 87.8 mm on 9 days in the observations. For July the ECMWF model produced 110 mm in 26 days, the observations yield 79 mm in 20 days. It has been found in earlier comparisons that the forecast systems tends to overestimate the number of convective rainfall events, specifically in the summer in the central U.S..

Daily averages of incoming solar radiation from the CTRL OI experiment have been computed and compared against in-situ observations (Figure 5). The overall agreement between the model and the observations is high; the correlation between both data sets is 0.85 and a small error of - 0.7 Wm^{-2} is present. Again, the period with the largest differences is the second half of June during which the model under-predicts the downward solar radiation. This is consistent with the overestimation of precipitation during this time.

Time series of top layer soil moisture for the CTRL OI experiment, the open loop run, and from the in-situ observations are shown in Figure 6a. Again, area averages for Oklahoma are presented; the temporal resolution is 6 hours. In general, the differences between the two model runs are rather small. However, the soil moisture analysis tends to add water especially during dry down periods. From 16 June to 21 June the dry down in both experiments results in a difference of 1.7 % volumetric soil moisture. Although the dynamic ranges of the model and the observations agree well, the differences between the model and the observations can be quite large, exceeding 5 % in mid-July. This is substantial given the fact that the dynamic range in the model does not exceed 10 %. These soil moisture differences are mainly caused by overestimation of modelled precipitation, but also by underestimation of solar radiation, which should result in too little evaporation. In addition, the model tends to dry out the soil too quickly, especially immediately after a strong rainfall event. Since the soil moisture analysis tends to add water the dry down rate at the surface seems to be slightly improved in the CTRL

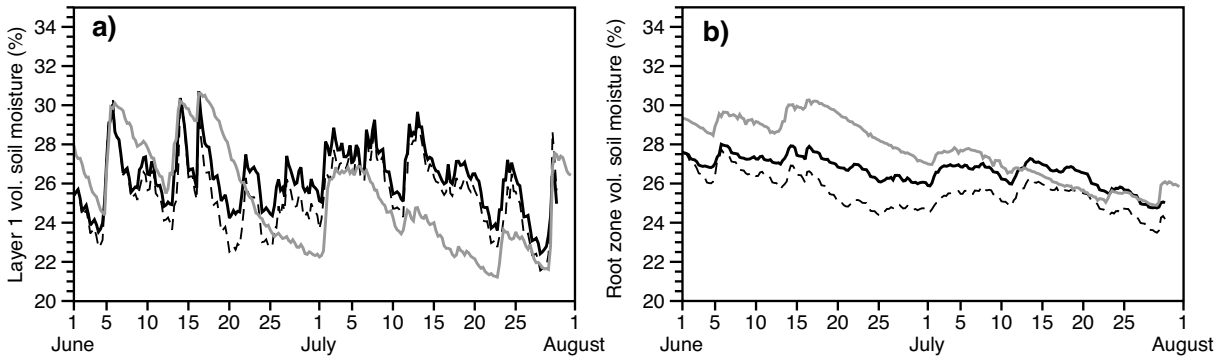

Figure 6: Analysed (black lines) and observed (grey line) soil moisture for the top soil layer and at 5 cm depth, respectively, (a) and for the root zone (1 m depth) (b) for the Oklahoma area. Results from the CTRL OI and OL experiments are shown as solid and dashed lines, respectively, at 6-hourly resolution.

experiment when compared against observations. However, the data assimilation system is not able to correct for the surface soil moisture errors introduced by a large rainfall error or the hydrological biases.

In the observed root zone soil moisture data the most significant signal is a slow dry down starting mid-June (Figure 6b). Observed values range from 30.5 % (mid-June) to 25 % (last week of July). Higher frequency temporal variability associated with the rainfall events during the first half of June is clearly visible but filtered; the amplitude is strongly reduced when compared against the surface soil moisture data. At the beginning of the study period, a significant bias between the model and the observations is present. This systematic difference can probably be attributed to deficiencies in the soil hydrology, i.e. too large values of hydraulic conductivity and the use of one soil type (Gedney et al., 2000; van den Hurk et al., 2002). Other potential sources for systematic differences are the absolute calibration of the sensors, which may not be perfect, and the choice of model soil properties. It is well known that the ECMWF TESSEL model (in contrast to HTESSEL, see Section 2) soil moisture has a rather small dynamic range defined through a permanent wilting point and a field capacity of 0.171 and 0.323 $m^3 m^{-3}$, respectively.

3.2.3 Issues concerning the interactions between analysis and assimilating model

In its current form, the operational soil moisture analysis is constrained by observations which are only weakly related to soil moisture. Effectively, soil moisture is a sink variable, in which errors introduced through the atmospheric forcing and the land surface model (TESSEL, in these experiments) accumulate. As a consequence the improved forecast performance in terms of low-level atmospheric parameters is not necessarily the result of more accurate soil moisture fields. As shown by Drusch and Viterbo (2007) it appears that the current soil moisture analysis procedure corrects the evaporation and heat fluxes at the surface, without producing improved soil moisture fields. These results are also confirmed by van den Hurk et al. (2008). One important step to address the situation was taken with the operational implementation of the improved land-surface hydrology in HTESSEL in November 2007 in the IFS cycle 32R3 (Section 2.1).

3.3 The Extended Kalman filter (EKF) surface analysis

To make optimal combined use of the conventional observations and future satellite measurements, an advanced surface data assimilation system has been implemented in the IFS and is currently being tested. The core of the system is a simplified extended Kalman filter (EKF), which is based on the idea of minimising a cost function

J as in variational methods. In addition the EKF accounts for the evolution of error covariances in time. The simulated soil moisture in the three root zone layers (state vector $\mathbf{x}$) is improved by minimising J optimally combining the information from model forecast of $\mathbf{x}$ and observed parameters (T_{2m}, RH_{2m}, and satellite derived soil moisture and / or brightness temperatures), and the observation vector $\mathbf{y}$:

$$J(\mathbf{x}) = (\mathbf{x}-\mathbf{x_b})^{\mathrm{T}}\mathbf{B}^{-1}(\mathbf{x}-\mathbf{x_b}) + (\mathbf{y}-H(\mathbf{x}))^{\mathrm{T}}\mathbf{R}^{-1}(\mathbf{y}-H(\mathbf{x})) \tag{2}$$

where H is the observation operator. For small dimension estimation problems, and under the tangent linear hypothesis, the minimum of J ($\nabla J = 0$) can be directly obtained through matrix manipulation. The solution for the analysed state at time t is:

$$\mathbf{x_a}(t) = \mathbf{x_b}(t) + \mathbf{K}_{[t,t+12]}\left(\mathbf{y}_{[t,t+12]} - \mathbf{H}_{[t,t+12]}\mathbf{x_b}_{[t,t+12]}\right) \tag{3}$$

with the gain matrix $\mathbf{K}$:

$$\mathbf{K}_{[t,t+12]} = \left[\mathbf{B}^{-1}(t) + \mathbf{H}^{T}(t)_{[t,t+12]}\mathbf{R}^{-1}\mathbf{H}(t)_{[t,t+12]}\right]^{-1}\mathbf{H}^{T}_{[t,t+12]}\mathbf{R}^{-1} \tag{4}$$

Here the gain matrix is expressed in model space rather than the usual formulation in observation space. Assuming a quasi-linear problem close to the background state, H can be approximated by a one-sided finite difference: one forecast run with perturbed initial conditions is then required for each state variable. H is calculated based on the difference between background and perturbed soil moisture of each layer and the difference of observed and modelled control variable at the time of the measurement. In this way, no adjoint or tangent linear models are needed. The background error covariance evolves in time according to:

$$\mathbf{B}(t+1) = \mathbf{M}_{t\rightarrow t+1}\mathbf{A}(t)\mathbf{M}^{T}_{t\rightarrow t+1} + \mathbf{Q}(t) \tag{5}$$

where $\mathbf{Q}$ is the model error covariance matrix and $\mathbf{M}$ is the tangent linear of the forecast operator M. We assume that the observation and model errors are mutually uncorrelated and white. $\mathbf{A}$ is the analysis error covariance calculated by:

$$\mathbf{A}(t) = [\mathbf{H}^{-1^{T}}(t)\mathbf{R}^{-1}(t)\mathbf{H}^{-1}(t) + \mathbf{B}^{-1}(t)]^{-1}. \tag{6}$$

In contrast to the original algorithm described by Hess (2001), we account for the soil water transfer between the soil layers by using perturbed model runs to estimate the tangent linear of the forecast operator $M_{t\rightarrow t+1}$. The start values of x_b for the following assimilation window (t+12) are calculated by:

$$\mathbf{x_b}(t+12) = M_{t\rightarrow t+12}\mathbf{x_a}(t) \tag{7}$$

The chosen 12-hour assimilation windows correspond to the 12-hour atmospheric 4D-Var analyses.

The EKF surface analysis as described above is computationally far more expensive than the OI. The main cost is the running of short-term perturbed forecasts to determine $\mathbf{H}$. These forecasts are currently conducted with the land surface model coupled to the atmosphere. Balsamo et al. (2007) have shown that perturbed simulations can be performed offline, ie with the land surface model decoupled from the forecasting model, without affecting the performances of the surface analysis. This result is confirmed by Mahfouf et al. (2008) which show that decoupling the surface model from the atmospheric model for the surface analysis makes the use of the Kalman filter affordable for operational applications. For future operational applications the ECMWF EKF surface analysis structure will be revised accordingly. First the surface analysis will be separated from the atmospheric 4D-Var and moved away from the critical time window. Second, the EKF surface analysis will be revised in order to perform the perturbed simulations with HTESSEL decoupled from the atmosphere, according to Mahfouf et al. (2008) and to Balsamo et al. (2007). This will also open the possibility to consider high spatial resolution for the perturbed simulations to make optimal use of vegetation and soil classification data sets and soil moisture analysis increments. Due to the large heterogeneity of these parameters any spatial interpolations should be avoided. In addition, a stand-alone version of the EKF surface analysis, where the surface model is fully decoupled from the atmosphere at all levels (perturbed and unperturbed forecasts), will be developed for research development and testing purposes.

3.4 Preliminary results from the EKF surface analysis

In order to evaluate the new surface analysis scheme we set up two data assimilation experiments. In agreement with the current surface analysis, both experiments use the screen-level parameters (2m temperature and relative humidity) to correct soil prognostic variables. The first experiment (OI), uses the operational soil moisture analysis. In the second experiment (EKF), the EKF surface analysis is used instead. Apart from the surface analyses scheme the experiments are identical and based on ECMWF's IFS cycle 33R1 coupled to the atmospheric 4D-Var analysis system. The horizontal resolution for the experiments is set to T159, the vertical resolution is set to 60 levels. All experiments start from the same initial (operational) model state at 1 May 2007, 0000 UTC and run for a 31 day period. A 6-hour assimilation window is used instead of the 12-hour window in the operational system in order to provide a more direct comparison with the OI experiment. In both experiments the observation errors are set to $\sigma_T = 2K$, $\sigma_{RH} = 10\%$. In this first test case the background error covariance matrix **B** is not cycled and its value is set constant to $\sigma_B = 0.01 m^3 m^{-3}$. Further experiments will be conducted in the very near future to account for the soil texture properties in the background error.

3.4.1 Jacobians of the Observation Operator

The observation operator H is the product of the model state evolution from time t_0 to time t_{obs} and the conversion of the model state into an observation equivalent. Thus the Jacobian **H** of the observation operator is expressed as:

$$\mathbf{H} = \frac{\delta y_{t_{obs}}}{\delta x_{t_0}} \tag{8}$$

The elements of the Jacobian matrix are estimated in finite differences by perturbing individually each component x_j of the control vector **x** by a small amount δx_j. A perturbed model integration allows the j-th column of this matrix to be constructed as:

$$H_{ij} = \frac{y_i(x + \delta x_j) - y_i(x)}{\delta x_j} \tag{9}$$

A sensitivity analysis is carried out to find the optimum perturbation δx_j. The tangent linear hypothesis suggests infinitesimal perturbations. However this does not necessarily lead to the best linear approximation of the observation operator. Balsamo et al. (2004) found that finite sized perturbations better satisfy the tangent linear hypothesis and addressed the reason for this behaviour to the influence of numerical and dynamical noise that becomes more important for smaller perturbations when the 2 m sensitivity is reduced. Figure 7 shows the difference between the Jacobians of T_{2m}, RH_{2m} with respect to the first three soil layers obtained with different perturbations (the perturbation amplitude δx_j is set to 0.0001, 0.0003, 0.0005, 0.001, 0.003, 0.005, 0.01, 0.03, 0.05). The results are plotted as global averages. To avoid spurious effects, we did not consider grid points where the soil moisture content was smaller/larger then the wilting point/field capacity. For these points a negative/positive perturbation would result in no signal and would lead to biased results. In a well behaved deterministic system, in the limit of small perturbation amplitude the Jacobians estimated with positive/negative perturbations should have similar values. Hence $h = (h_1^+ + h_1^-)/2)$ should be constant and $|h_1^+ - h_1^-|$ should tend to zero. As in Balsamo et al. (2004) this is only the case for finite perturbations of 0.01 $m^3 m^{-3}$. Accordingly a value of $\delta x_j = 0.01$ $m^3 m^{-3}$ is used for the three soil moisture layers analysed. For infinitesimal and for large perturbation $|h_1^+ - h_1^-|$ tends to be larger than zero suggesting that the tangent linear assumption is not fulfilled. The sensitivity of T_{2m} (RH_{2m}) with respect to soil moisture is mostly negative (positive) which means that an increase in soil moisture will reduce (increase) the value of the screen level temperature (relative humidity).

The mean values of the Jacobians for T_{2m}, RH_{2m} are larger for the surface layer than for the root zone layers. It means that the assimilation will be more effective in modifying the surface layer in order to fit the observations

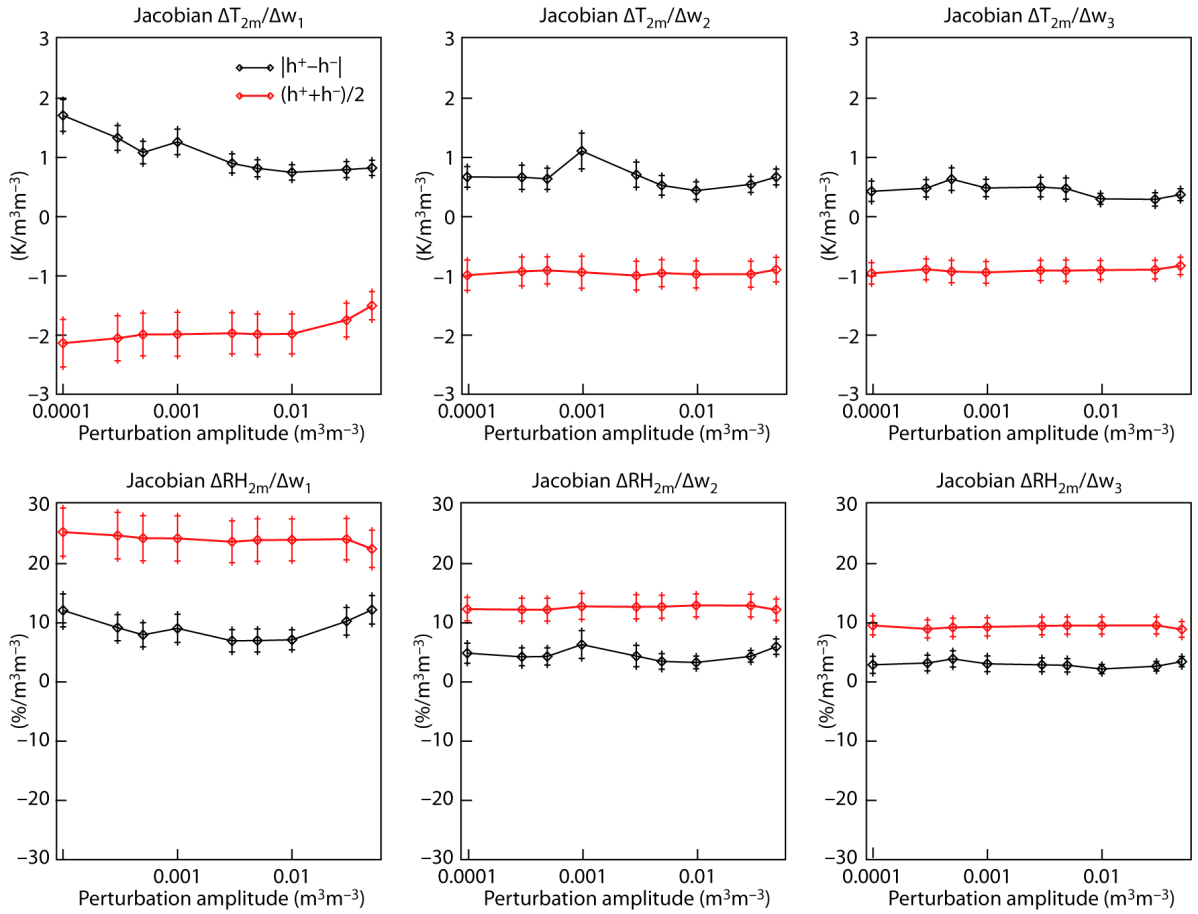

Figure 7: Examination of the elements of the Jacobian matrix of the observation operator. The plots show the average $(h = (h_1^+ + h_1^-)/2)$ *and the absolute difference* $(|h_1^+ - h_1^-|)$ *of the* T_{2m} *(top) and* RH_{2m} *(bottom) components calculated for positive* (h_1^+) *and negative* (h_1^-) *perturbations as a function of perturbation size for the uppermost three soil layers (top: 0.07 m; middle: 0.21 m; bottom: 1m; soil layer).*

than in modifying the root zone soil moisture. For the T_{2m}, RH_{2m} this might be surprising and it is in contrast to Mahfouf et al. (2008) who found a larger sensitivity of the root zone for the ISBA land surface scheme used at Météo-France. This is explained by the conceptual differences between the two land surface schemes. The ISBA model uses a force-restore approach which link empirically the surface layer (1cm) and the root zone soil moisture, but there is no physical diffusion from the surface to the root zone. In contrast HTESSEL uses a physical formulation to describe the soil infiltration and capillary diffusion processes. Accordingly, variablity and amplitude of variations are attenuated through diffusion processes, in the root zone compared to surface layer. In our experiment we use a short assimilation window which limits sensitivity with respect to the deeper layers. The operational 12-hour window will be more suitable for our physically based soil water diffusion scheme in order to ensure the propagation of the perturbations through the root zone.

3.4.2 Gain Components

The most relevant aspect to assess differences between the OI and the EKF surface analyses are the gain matrix elements which are computed analytically and dynamically, respectively. To analyse the gain matrix elements we use the same setup as before. The elements of the Jacobian matrix are estimated, by perturbed runs (one for

each soil layer analysed) with a soil moisture perturbation of 0.01 m^3m^{-3}. To avoid spurious corrections the soil moisture analysis is locally switched off if the Jacobian becomes larger then $50K/m^3m^{-3}$ or $5/m^3m^{-3}$ for the T_{2m} or RH_{2m} component respectively. This mainly occurs in specific areas (North Sahara, Central Australia) when very low values of RH_{2m} are observed and very low soil moisture is simulated, leading to a high sensitivity of the Jacobian to the soil moisture perturbation. In addition, the analysis is switched off if the soil moisture increment for any layer is larger than $0.1m^3m^{-3}$.
Figure 8 and Figure 9 show the T_{2m} and RH_{2m} gain components for the 12UTC analysis (01 May 2007) from the OI and EKF experiments, respectively. Results are presented for one day to illustrate the difference between the OI and the EKF soil moisture analysis. Using only one day ensures the clarity of the results (no averaging or sum effects) and also allows to compare our results to those obtained by Mahfouf et al. (2008). Gain coefficients are expressed in $\%m^3m^{-3}/K$ for the T_{2m} component and in $\%m^3m^{-3}$ for the RH_{2m} component (RH_{2m} being expressed as a non-unit fractional value). As already shown by Mahfouf et al. (2008), the RH_{2m} gain components are about one order of magnitude larger than the T_{2m} gain coefficients, for both the OI and the EKF experiments. They exhibit similar patterns in Figure 8 and in Figure 9, with low values over mountainous areas, in presence of snow, freezing temperatures and in desert areas. The OI and EKF coefficients also depict a strong diurnal cycle. In the OI formulation this dependency is controlled by accounting for the solar zenith angle in the gain function. This is clearly visible in the OI gain component (Figure 8) which is limited to the region between 20°W and 130°E. In the EKF there is no explicit relationship between the gain and the solar zenith angle or other rejection criteria. The link between the screen level and soil variables is provided through turbulent surface fluxes, leading to a diurnal cycle based on physical processes. Thus, in contrast to the OI experiment, the assimilation is not switched off at night in the EKF and for the 12UTC analysis low values of gain coefficients are allowed over America and Australia.

In agreement with Mahfouf et al. (2008), the gain coefficients are lower by a factor 2 to 4 between OI and EKF for both the T_{2m} and the RH_{2m} components. In addition, the relative amplitude of the coefficients for the different soil layers is represented in the EKF only. In the OI analysis the gain coefficients are similar for all layers. They express the gain in term of volumetric soil water content. Since the thickness of the soil layers increases with the soil depth, much larger gain are computed for deep soil layers than for surface layers when absolute soil water content are considered (integrated over depth). This leads to unrealistic large values of gain coefficients at depth. With the EKF surface analysis, relatively large coefficients are found for the uppermost soil layer, and they decrease with the soil layer depth. In this aspect the EKF better reflects the sensitivity of the different layers to the surface fluxes.
Low values of EKF gain coefficients over the tropical rain forest and in high latitudes highlight the ability of the EKF in automatically masking situations where the soil moisture is not strongly linked to the near-surface atmosphere (e.g. close or passed field capacity), while the OI coefficients (having no dependency on soil moisture state) are significantly larger. These features however need further investigations to be fully validated.

3.4.3 Soil Moisture Increments

The amplitude and evolution of the analyses increments are a useful diagnostic of the forecast system. A well calibrated, physically sound model is characterised by small, randomly distributed analysis increments. As previously mentioned, large and/or persistent increments indicate systematic model and/or observations errors. Considering that the analysis of the OI experiment effectively corrects model deficiencies (Section 3.1), and that we use the same forecast model in the data assimilation experiments, we expect similar spatial and temporal patterns in the mean analysis increments. Figure 10 shows analysis increments from the OI and EKF experiments (01 May 2007, 12UTC). Increments obtained in the EKF experiment show similar spatial patterns to those from the OI experiment. But in contrast to the OI, substantial EKF increments are allowed over the

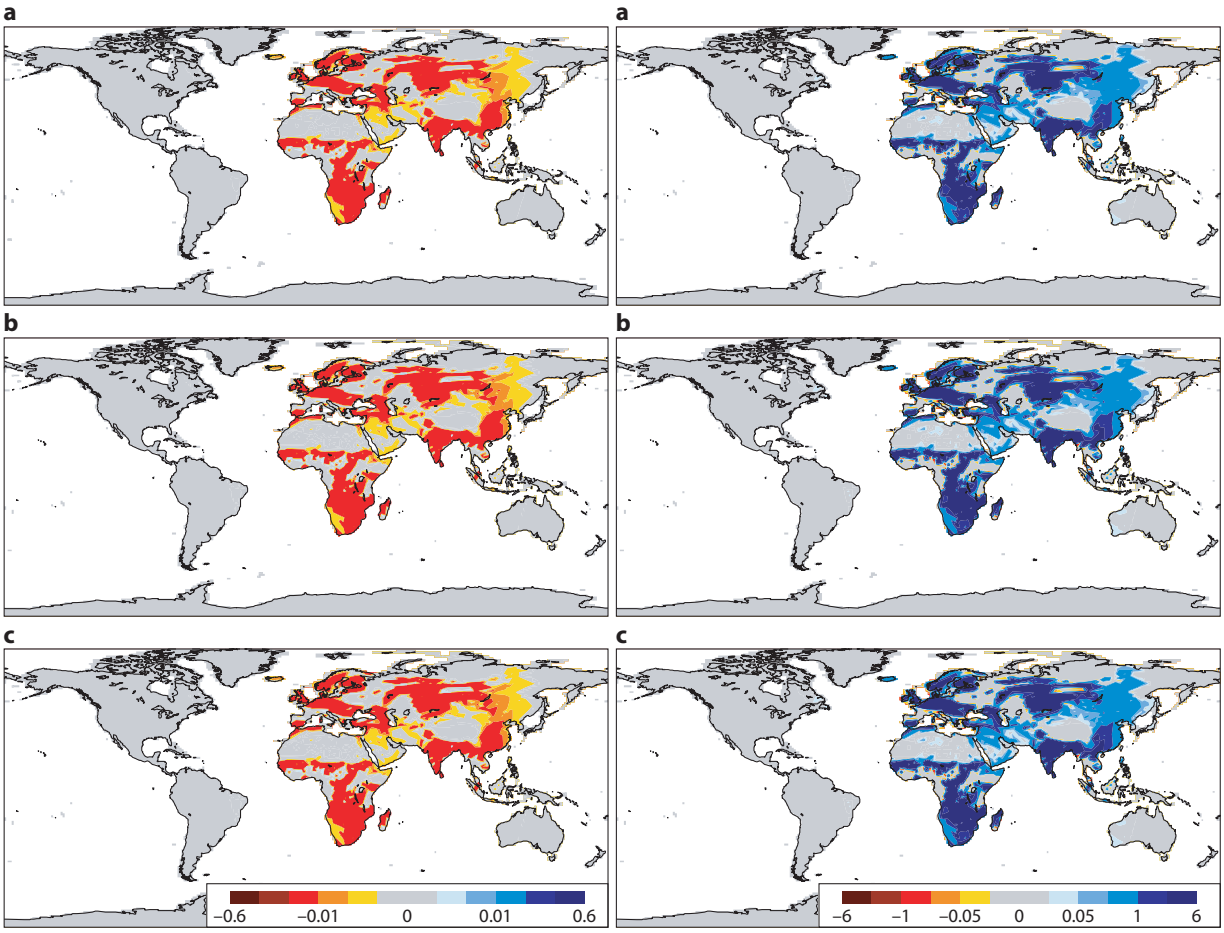

Figure 8: Gain matrix coefficients from the OI analysis for the T_{2m} (left) and the RH_{2m} (right) components (01 May 2007, 12UTC). The gain coefficients are expressed in $\%m^3m^{-3}/K$ and in $\%m^3m^{-3}$ for T_{2m} and RH_{2m} respectively. Panels a, b, c refer to the top (0-0.07m), middle (0.07-0.28m) and bottom (0.28-1m) soil layers respectively.

American and Australian continents in agreement with gain matrix the EKF coefficients. Over Europe and Asia and Africa they are smaller than for the OI, particularly for the sub surface layers. Reduced analysis increments at depth as to be regarded as a positive effect for the hydrological consistency.

4 Active Microwave

4.1 MetOp and ERS scatterometers

Although designed to measure wind over the ocean, it is now clear that the ERS and MetOp scatterometers also provide valuable information on surface soil moisture over land. These are active microwave instruments operating in the C-band (5.6 GHz) at VV polarisation. ERS-1 was operated between August 1991 and May 1996. ERS-2 was launched in March 1996 and was operated until January 2001, when due to a failure of a gyroscope all ERS-2 instruments were temporarily switched off. Since May 2004, ERS-2 again acquires data and is foreseen to operate until 2011. However, the down-link of data is limited to specific regions (i.e. North America, Europe, Northwest Africa, China and Australia). An operational continuation of the scatterometer missions is since November 2006 provided by the ASCAT instrument on the European MetOp-A satellite.

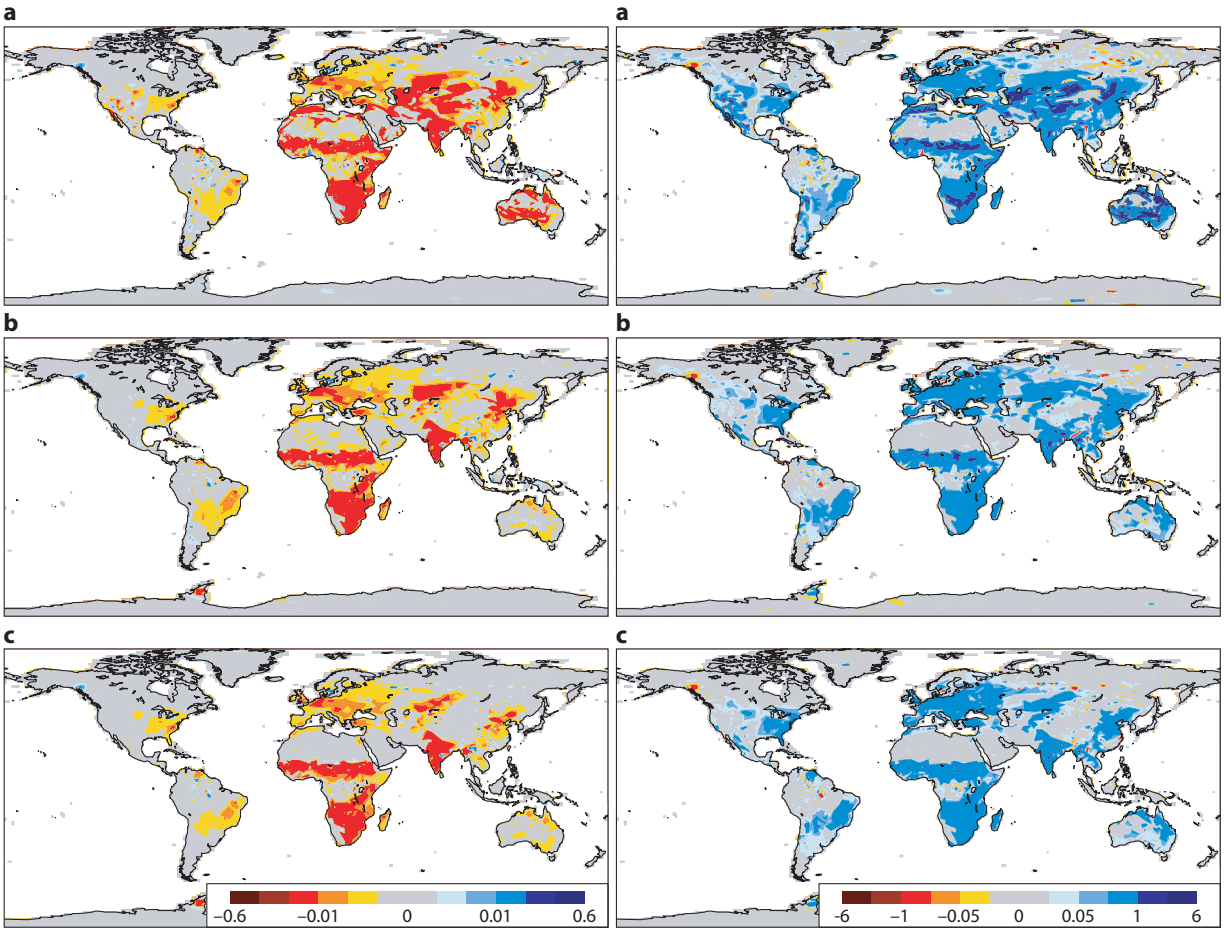

Figure 9: Gain matrix coefficients from the EKF analysis for the T_{2m} (left) and the RH_{2m} (right) components (01 May 2007, 12UTC). The gain coefficients are expressed in $\%m^3m^{-3}/K$ and in $\%m^3m^{-3}$ for T_{2m} and RH_{2m} respectively. Panels a, b, c refer to the top (0-0.07m), middle (0.07-0.28m) and bottom (0.28-1m) soil layers respectively.

Since June 2008 EUMETSAT are operating near-real time soil moisture processor at its central processing facility. The processor retrieves a soil moisture index w_s based on the TUWien model described in Wagner et al. (1999). Based on ERS scatterometer data it was shown in several validation studies that w_s contains skilful information about soil moisture (Wagner et al., 2003; Dirmeyer et al., 2004; Crow and Zhan, 2007). These studies provide qualitative comparisons between w_s and different datasets, showing good agreement for tropical, dry and temperate regions. Disagreements were found in deserts and polar regions. In a more quantitative study, Ceballos et al. (2005) compared root-zone soil moisture derived from w_s with in-situ data from a field site in central Spain and estimated a root mean square error (RMSE) of 0.04 m^3m^{-3}. In a similar study using in-situ observations from agro-meteorologic networks in Russia, Ukraine and China, Scipal (2002) estimated a RMSE of 0.06 m^3m^{-3}. Recently, w_s was also used successfully in first agro-meteorologic assimilation experiment (de Wit and van Diepen, 2007) and in hydrological (Parajka et al., 2006; Scipal et al., 2005), meteorological and climate (Zhao et al., 2006) studies. Initial soil-moisture retrieval tests, based on ASCAT observations, indicate that the advanced sensor design and calibration provides accurate soil moisture information at a spatial resolution of 25 km and a sampling interval of less than two days (Bartalis et al., 2007). The MetOp system will hence provide an uninterrupted source of soil-moisture information until at least 2020.

Scatterometers operating in the low frequency domain (1–10 GHz) provide a relatively direct measure of soil moisture because of their high sensitivity to the water content of the top soil layer. The challenge in retrieving

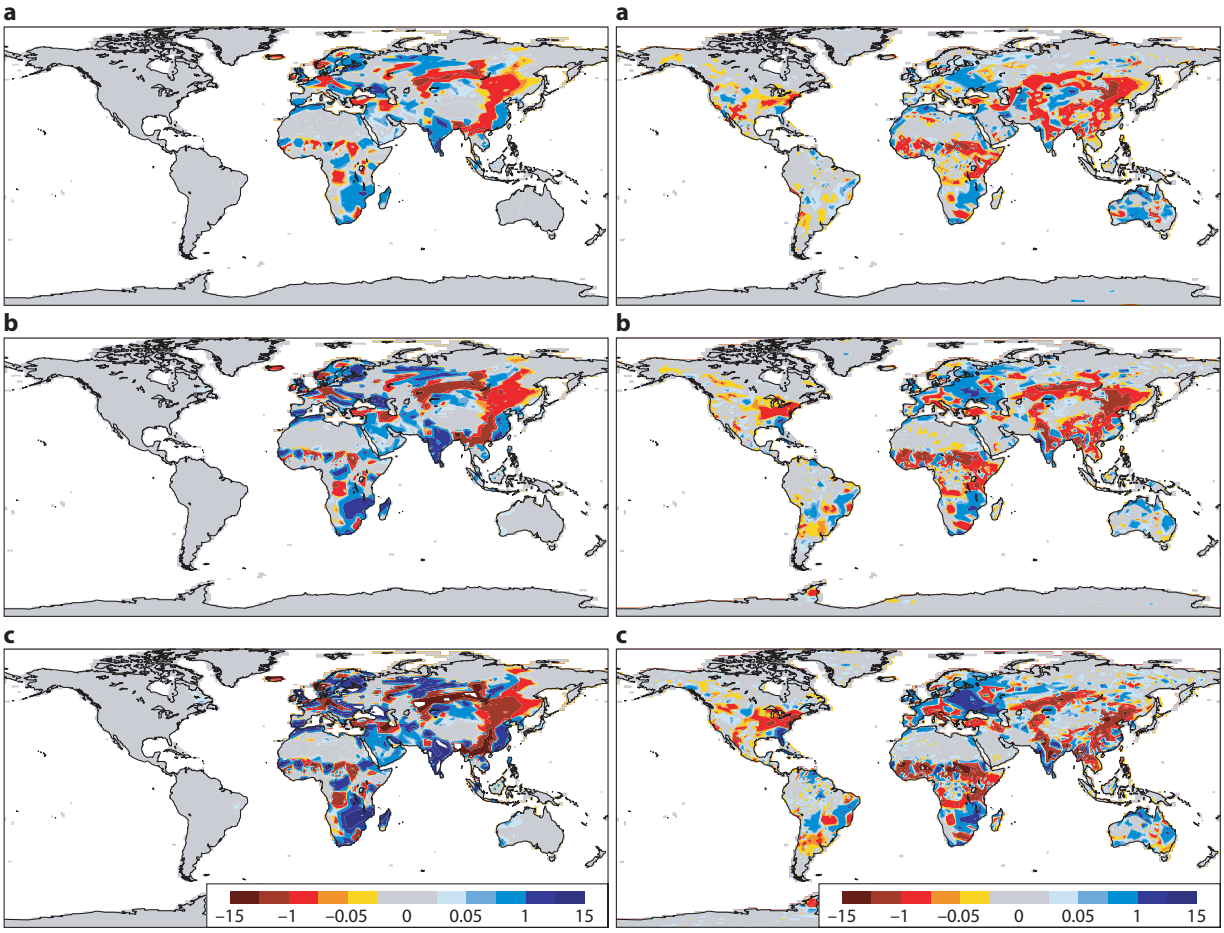

Figure 10: Analysis increment (in mm) from the OI (left) and EKF (right) experiments (01 May 2007, 12UTC). Panels a, b, c refer to the top (0-0.07m), middle (0.07-0.28m) and bottom (0.28-1m) soil layers respectively.

soil moisture from the backscatter measurement σ^0 is to account for the effects of surface roughness and vegetation. To this end, the TUWien model exploits the unique sensor design and the advantages of a change-detection method. To correct for the effects of plant growth and decay the model uses the vegetation sensitive signature of the multi-incidence angle σ^0 observations. The soil moisture index w_s is then retrieved by relating the instantaneous, vegetation-corrected σ^0 observation to a wet (σ^0_{wet}) and dry (σ^0_{dry}) reference. The resulting quantity is a relative measure of surface (< 2 cm) soil moisture ranging between 0 and 1. Assuming that σ^0_{dry} represents a completely dry and σ^0_{wet} a saturated soil surface, w_s is equal to the degree of saturation, which is the soil-moisture content expressed in percent of porosity. The reference values σ^0_{dry} and σ^0_{wet}, are estimated from the lowest and highest σ^0 values recorded during the period August 1991 to January 2001. By utilising data from a nine-year period, the reference values likely represent the respective soil conditions even in sparsely sampled areas. In extreme climates such as deserts, where saturation is not observed, a correction factor is applied to σ^0_{wet} in order to obtain spatially consistent w_s values.

It is important to note that the method does not provide useful information if the signal is dominated by scattering from dense vegetation, water, rough topography or snow covered/frozen land surfaces. Additionally, the current implementation of the TUWien model does not explicitly incorporate azimuthal viewing effects as they are generally weak. In regions characterised by surface patterns with a distinct azimuthal orientation of the micro relief, e.g. in sand deserts, this simplification however results in an artificial modulation of the signals.

To avoid the use of spurious information, w_s undergoes a rigorous data screening. The screening rejects data if the observation error of w_s exceeds 6%. In this context, the observation error refers to the propagation of instrument noise through the soil moisture retrieval model and depends on the location-specific sensitivity of the microwave signal to soil moisture, to instrument noise, azimuthal viewing effects and speckle. It is the smallest expected error, assuming that the assumptions made in the TUWien model are correct. Additionally, we used the Global Lakes and Wetlands Data Base Lehner and Döll (2004) to mask regions where the areal fraction of water surfaces exceeds 15% of the scatterometer footprint. Global digital elevation data from the GTOPO30 data set was used to mask regions where the normalised elevation variation within a scatterometer footprint exceeds 20%.

4.2 Comparison of ERS and ERA-40 soil moisture

To determine if w_s and the ECMWF model capture the same physical process, we calculated the linear correlation (R_{ABS}) between w_s and soil moisture data (Θ_E) from the ECMWF 40-year re-analysis (ERA-40) from the period 1992–2000 (Scipal et al., 2008). To obtain matching data sets we aggregated w_s to the ERA-40 grid and pooled it into six-hourly files. Observations were masked if one of the datasets indicated missing observations or if the ERA-40 re-analysis indicated a screen level temperature below 0°C and/or a snow depth larger than 0 mm. Considering the strong seasonality of soil moisture in certain regions, R_{ABS} has to be interpreted carefully. In the Monsoon areas for example, R_{ABS} will be dominated by a strong seasonal variation, suppressing soil-moisture anomalies which occur with a much weaker amplitude. We therefore also calculate the anomaly correlation (R_{ANO}). These are obtained by removing the mean seasonal cycle in w_s and Θ_E as derived from the nine year reference period. Although the nine year period is too short to calculate a robust climatology it allows us to remove the dominating effect of the seasonal cycle. The calculation of anomalies is based on a temporally identical population, i.e. if either w_s or Θ_E is missing for a specific time the corresponding value is removed from the other dataset. Comparing the two datasets does not provide any quantitative information about the quality of the data. However, considering that both datasets are fully independent we assume that a high correlation indicates that the same processes are captured. This assumption is valid also because the main simplifications in the model (e.g. a uniform soil type) and in the satellite retrieval will have a de-correlating effect.

Figure 11 shows the spatial distribution of R_{ABS} and R_{ANO}. In general, R_{ABS} is positive over large parts of the land surface, with maximum values around 0.9. At 85% of the land points the correlation R_{ABS} is significant at the 0.05 level, at 8% of the land points soil moisture is not correlated significantly and at 7% the correlation is negative at the 0.05 confidence level according to a t-test. For R_{ANO} these figures are similar. The spatial distribution of R_{ABS} clearly reflects zonal climate patterns. As expected, R_{ABS} is high in areas characterised by a strong seasonal soil moisture cycle, for example in monsoon regions. For these areas, R_{ANO} has lower values than R_{ABS}, especially over Africa where R_{ANO} is around 0.3 while R_{ABS} is around 0.9. A possible explanation is a deficiency in the model, which can hardly be corrected through the operational analysis considering the lack of synoptic in-situ observations. Over deserts R_{ABS} becomes negative. This problem has been reported previously by Wagner et al. (2003) and can be attributed to a shortcoming of the TUWien model. The maps also exhibit some unexpected features. Over Europe, R_{ABS} and R_{ANO} are comparably high. Similarly, R_{ABS} and R_{ANO} are high over southeast China despite a relatively high amount of above-ground biomass. In a study using soil moisture data derived from the AMSR-E radiometer, which operates in the same microwave band, the area was masked as the observations did not contain skilful information (Reichle et al., 2007). On the other hand, R_{ABS} is comparably low over the eastern parts of North America. The reason for these low correlations are not yet fully understood but can possibly be related to higher amounts of above-ground biomass and hence to a higher level of noise in w_s. Nevertheless, there is general agreement between Θ_E and w_s and both datasets seem to capture the fundamental soil moisture processes. This results is consistent with the study of Dirmeyer

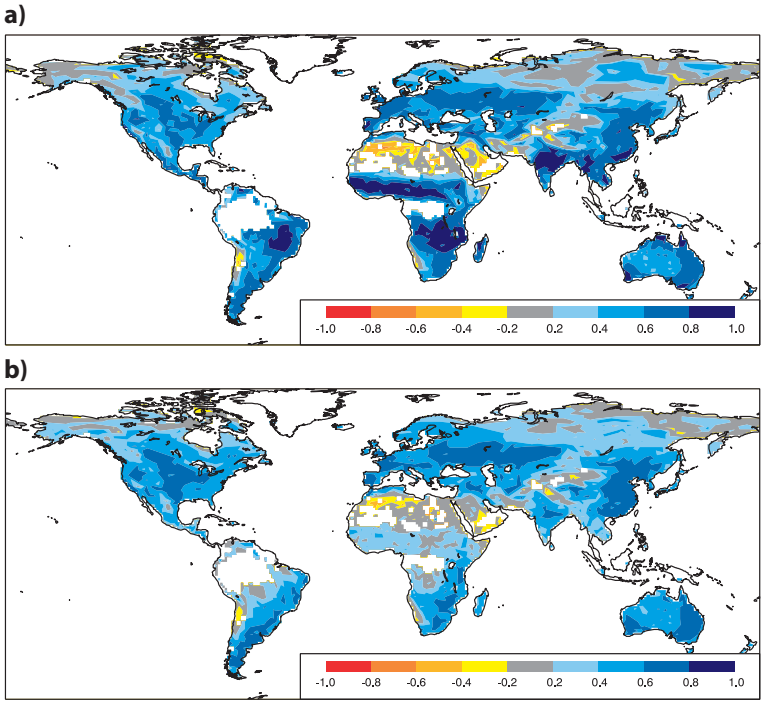

Figure 11: Correlation between the scatterometer derived soil moisture index w_s and ERA-40 reanalysis soil moisture Θ_E for (a) absolute values (R_{ABS}) and (b) anomalies for the period 1991 to 2001 (R_{ANO}).

et al. (2004) which showed good performances of the ERA-40 and the ERS soil moisture products.

4.3 Observation Operator

Assuming that w_s reflects the degree of saturation, model equivalent volumetric soil moisture can be derived by a rescaling with the model value of porosity, which is a prescribed quantity. However, such a transformation does not account for shortcomings of the model physics and the satellite retrieval method, which can result in large biases especially in the mean and variance. Therefore, we transform w_s with respect to the climatology of the model. To this end we use soil moisture data (Θ_E) from ERA-40 from the period 1992-2000. The transformation is accomplished by scaling w_s so that the cumulative distribution functions (CDF) of w_s and Θ_E match. In similar studies, (Drusch et al., 2005; Drusch, 2007), the data transformation was achieved by ranking datasets of satellite derived and model soil moisture and fitting a 3^{rd} order polynomial to the differences. This approach corrected the differences in the mean, the variance, the skewness and the kurtosis. Here, we simplified the CDF matching to a linear transform. This effectively removes the differences in the first two moments (mean and variance). Differences in higher-order moments are mainly found in dry climates. In these regions, Θ_E is more skewed towards dry values and shows a narrower distribution (i.e. a higher kurtosis). These higher-order differences will enter the assimilation as an uncorrected bias. The impact of ignoring differences in higher-order moments is nevertheless small and scarcely reaches values larger than 0.02 m^3m^{-3}. The disadvantage of neglecting differences in higher moments is, however, compensated by the robustness of the method especially in data sparse regions. The linear approach is also attractive as it can be fully parameterised by the mean and variance of Θ_E and w_s. The transformed soil moisture index w_s^* is then expressed as:

$$w_s^* = a + b \cdot w_s \quad \text{with}$$

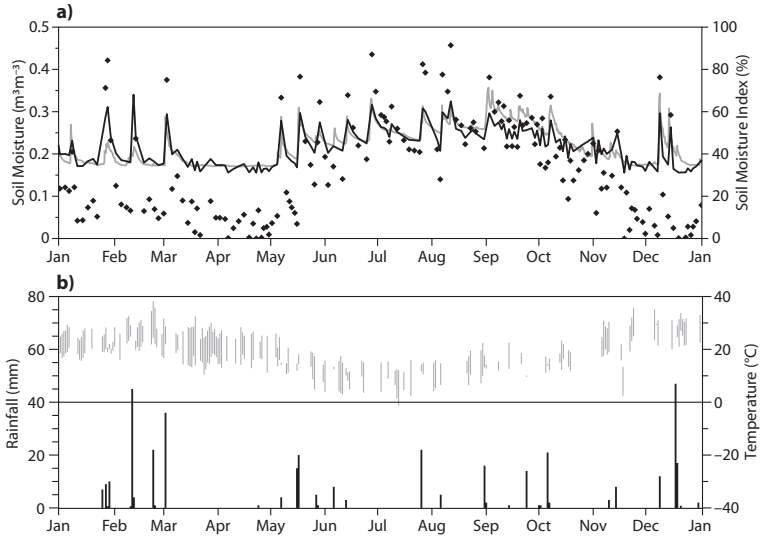

Figure 12: (a) ERS scatterometer derived soil moisture index w_s (diamonds, right x-axis scale), transformed soil moisture index w_S^* (black line) and model soil moisture Θ_E from the ERA-40 reanalysis (grey line) in eastern Australia (34.3°S/148.8°E). (b) Observed rainfall and temperature range at the nearby synoptic weather station Frogmere.

$$a = \overline{\Theta}_E - \overline{w}_s \cdot \sqrt{\frac{VAR(\Theta_E)}{VAR(w_s)}}, \quad b = \sqrt{\frac{VAR(\Theta_E)}{VAR(w_s)}} \tag{10}$$

where *VAR* denotes the variance and the bar denotes the mean of the respective sample. The intercept a and slope b are local coefficients depending on factors such as soil type, land cover and climate. Therefore, the coefficients are derived for each model grid-box independently. Spatial averaging was also omitted to minimise ergodicity errors (Reichle and Koster, 2004).

Figure 12 shows an exemple of a time series of w_s, w_s^* and Θ_E for a grid point in eastern Australia (34.3°S/148.8°E) for a one-year period. Generally, w_s and Θ_E capture variations induced by rainfall events observed by the nearby synoptic weather station Frogmere well. Both datasets also agree in the dry down rates. w_s shows a higher noise level, which is especially evident during the long dry spell in April. After applying Equation 10 differences in the dynamic range of w_s and Θ_E are reduced, and w_s^* is almost bias free with respect to Θ_E.

It has to be noted that in November 2007 a new soil hydrology (HTESSEL) was implemented in the surface scheme (Section 2.1). This change results in a different climatology than the ERA-40 climatology which is based on TESSEL. Until sufficient data is available to re-calibrate the transfer function (Equation 10) a simple rescaling based on the new soil hydrologic properties (wilting level, and field capacity) is in use.

4.4 Preliminary Assimilation Results

To evaluate the impact of the scatterometer-derived soil moisture data on the soil moisture analysis and the weather forecast we performed a data assimilation experiment. The experiment is based on the same setup as used in Section 3.4 with the difference that the ASCAT soil moisture observations are used in the EKF surface analysis (EKF-ASCAT experiment). In this preliminary study the observation error is set to $0.02 m^3 m^{-3}$.

4.4.1 *Jacobians of the Observation Operator*

Similar to Section 3.4 we performed a sensitivity analysis to find the optimum perturbation for the soil moisture Jacobians. For direct soil moisture observations $|h_1^+ - h_1^-|$ is approximately zero over the entire perturbation range and the sensitivity, expressed in $h = (h_1^+ + h_1^-)/2$ is positive. As for the previous EKF experiment presented in this paper, a small perturbation value of $\delta x_j = 0.01\ m^3.m^{-3}$ is used for the EKF-ASCAT experiment. The mean values of the Jacobians obtained for the top soil layer (0-7cm) are close to 1; whereas the Jacobians for the second soil layer and for the third soil layer are negligible ($0.02 m^3 m^{-3}/m^3 m^{-3}$ and $0 m^3 m^{-3}/m^3 m^{-3}$). This indicates that, based on the experimental setup, the assimilation will only lead to substantial modifications of the surface layer and soil water has to be propagated to deeper layers via infiltration.

4.4.2 *Gain Components*

Figure 13 (left) shows the mean gain component w_s (01-03 May 2007, 12UTC). A 3-days period is considered to have a substantial coverage. This allows comparing EKF-ASCAT to the 1-day results obtained from the previous experiments based on screen level parameters (previous section). Since there is a direct link between the observations and the analysed fields the EKF coefficients do not depend on the time of the day. Gain values are the same order of magnitude over Europe (day time) and Australia and South America (night time). As for the screen level parameters assimilation using the EKF surface analysis (Figure 9), low values of the gain are obtained at high latitudes and in regions of dense vegetation. Over the tropics, in deserts and under snow/freezing conditions ASCAT soil moisture observations are not available and the gain therefore is zero.

4.4.3 *Soil Moisture Increments*

Figure 13 (right) shows the mean analysis increment of the EKF-ASCAT experiment (01-03 May 2007, 12UTC). This figure indicates that the surface layer increments have the same order of magnitude when the ASCAT data and the screen level parameters are assimilated. But the second and third soil layers increments are of lower amplitude with the EKF-ASCAT experiment than with the EKF experiment which considers screen level parameters (previous section). When averaged over one month (not shown), similar patterns and amplitudes between the EKF-ASCAT increments and the increments obtained with the OI and the EKF analyses (Section 3.3) are obtained for temperate and low latitudes. But at high latitudes EKF-ASCAT increments are much higher than those obtained when screen level parameters are used for the soil moisture analysis. This shows the potential of ASCAT data assimilation for the high latitude soil moisture analysis. Further work is necessary to investigate in depth the impact of using ASCAT data in the soil moisture analysis and to compare the results with those obtained when screen level parameters are used.

4.4.4 *Forecast Impact*

The global scale impact of the new EKF surface analysis is neutral when screen level parameters or ASCAT data are assimilated. Performances in terms of 1000 hPa temperature indicate however variations in regional scale performances of the new EKF system. For example over North America the RMSE are slightly lower (by about 0.1K) for the EKF-ASCAT scheme than for the OI scheme. Further investigations are required to quantify the EKF surface analysis performances at different temporal and spatial scales and to generalise these preliminary results.

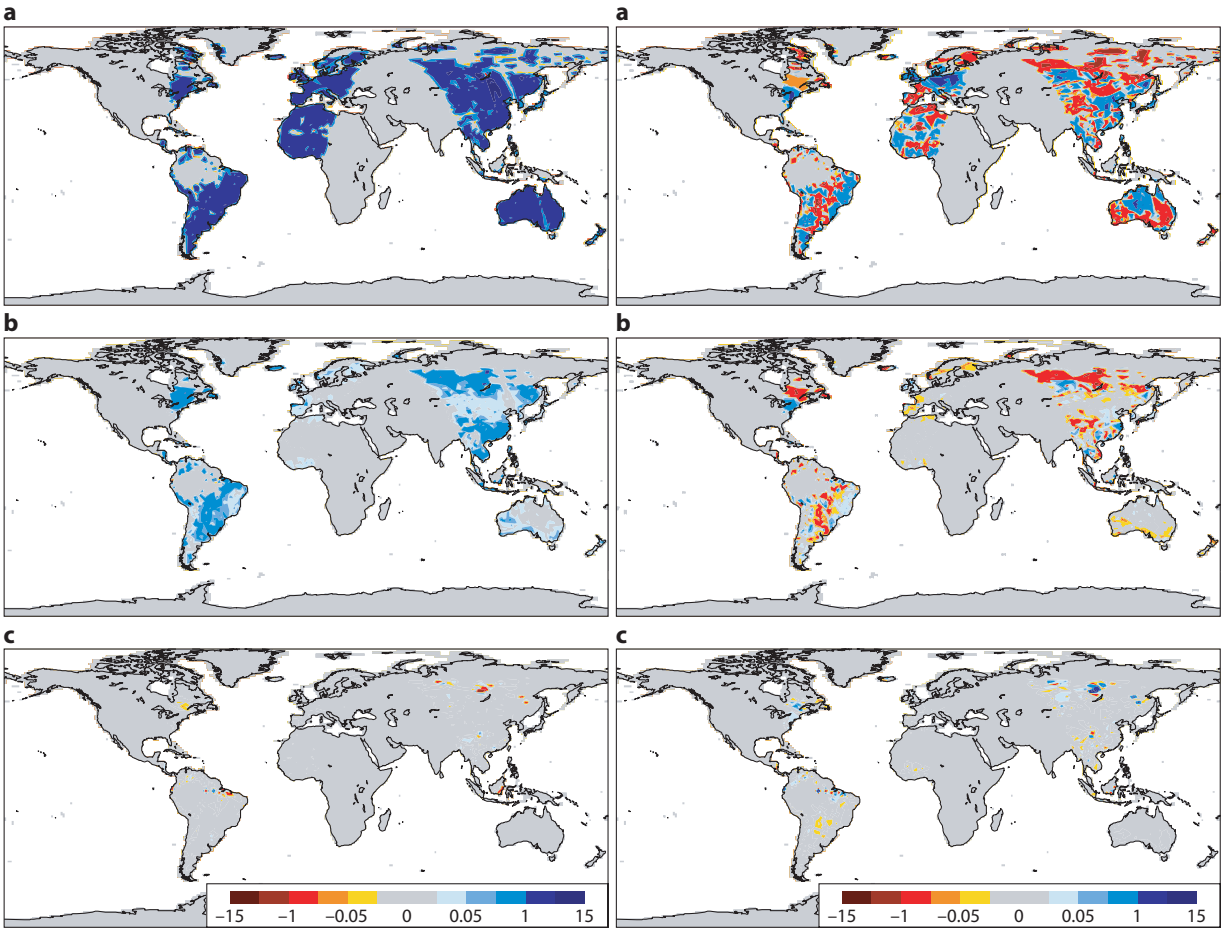

Figure 13: Gain matrix coefficients (left) and analysis increment (right) from the EKF-ASCAT experiment (mean values for 01-03 May 2007, 12UTC). The gain is expressed in $\%m^3m^{-3}/m^3m^{-3}$ *(*$\times$ *10) and the increment is in mm. Panels a, b, c refer to the top (0-0.07m), middle (0.07-0.28m) and bottom (0.28-1m) soil layers respectively.*

5 Passive Microwave

Passive microwave remote sensing is the most promising approach for the global monitoring of surface soil moisture (e.g. Njoku et al., 2003; Kerr et al., 2001). At low frequencies below 5 GHz microwave radiation penetrates the atmosphere and clouds so that the atmospheric contribution to the emission is almost negligible (e.g. Njoku et al., 2003). The effects of soil roughness and of the attenuating vegetation layer on the observations are small compared to measurements at frequencies exceeding 19 GHz.
Passive microwave remote sensing of soil moisture uses the strong contrast between the soil matrix dielectric constant and the water dielectric constant (4 and 80, respectively). The surface dielectric constant increases with the soil moisture content leading to an increase of the surface reflectivity; therefore, the surface emissivity and the brightness temperature decrease when soil moisture increases.

The future European Space Agency's SMOS (Soil Moisture and Ocean Salinity) Earth Explorer, to be launched in spring 2009, will be the first mission specifically devoted to remote sensing of soil moisture over land (Kerr, 2007; Kerr et al., 2001). The mission will provide interferometric measurements of multi-angular, bi-polarised brightness temperatures at L-band in near-real time. ECMWF plays a major role in preparing the use of SMOS brightness temperatures by the NWP community.

ECMWF's contribution to the SMOS mission is two-fold: first, a data monitoring system for the SMOS near real time product is being developed to provide a timely quality check for ESA and the SMOS calibration and validation teams. Second, SMOS brightness temperature data will be assimilated in ECMWF's global NWP system to quantify the impact of this new observation type on the forecast quality. One main component of the monitoring and of the surface data assimilation system is the observation operator that transforms model fields (soil moisture and ocean salinity) into observation space (brightness temperatures).

In the following sub-sections we describe the observation operator and perform an initial calibration using historical data from the NASA Skylab mission and from ERA-40 climate reanalyses. Furthermore, within the framework of the AMMA (African Monsoon Multidisciplinary Analysis) project we evaluate the applicability of the observation operator to AMSR-E observations at C- and X-band.

5.1 The CMEM Low-frequency Observation Operator

The Community Microwave Emission Model (CMEM) has been developed by ECMWF as the forward operator for low-frequency passive microwave brightness temperatures at 1 to 20 GHz (http://www.ecmwf.int/research/ESA_projects/SMOS/cmem/cmem_index.html). The physics is based on a simplified solution of the vector radiative transfer equation; in addition, it comprises parameterisations used in the L-Band Microwave Emission of the Biosphere model (L-MEB, Wigneron et al., 2007) and the Land Surface Microwave Emission Model (LSMEM, Drusch et al., 2001). CMEM's modularity allows different parameterisations to be considered for the main components.
For the atmospheric radiative transfer calculations, the RTTOV (Saunders et al., 1999) software package will be used. RTTOV is updated and maintained by the UK Met Office and ECMWF under the framework of EUMETSAT's NWP-SAF. Although CMEM has been designed for frequencies below 20 GHz, its modular structure allows future upgrades to higher frequencies and applications in the atmospheric 4D-Var analysis system.
For polarisation p the brightness temperature over snow free areas at the top of the atmosphere $T_{Btoa,p}$ can be expressed as:

$$T_{Btoa,p} = T_{Bau,p} + exp(-\tau_{atm,p}) \cdot T_{Btov,p} \tag{11}$$

and

$$\begin{aligned} T_{Btov,p} &= T_{Bsoil,p} \cdot exp(-\tau_{veg,p}) \\ &+ T_{Bveg,p}(1 + r_{r,p} \cdot exp(-\tau_{veg,p})) \\ &+ T_{Bad,p} \cdot r_{r,p} \cdot exp(-2 \cdot \tau_{veg,p}) \end{aligned} \tag{12}$$

where $T_{Bau,p}$ (K) is the up-welling atmospheric emission and $\tau_{atm,p}$ is the atmospheric optical depth. $T_{Btov,p}$ (K) is the top of vegetation brightness temperature when the vegetation is represented as a single-scattering layer above a rough surface. $T_{Bsoil,p}$ (K), $T_{Bveg,p}$ (K) and $T_{Bad,p}$ (K) are the soil, vegetation layer and downward atmospheric contributions, respectively. $r_{r,p}$ is the soil reflectivity of the rough surface (one minus the emissivity $e_{r,p}$) and $\tau_{veg,p}$ is the vegetation optical depth along the viewing path. The contribution emitted from the soil can be written as the product of the soil emissivity $e_{r,p}$ and the effective temperature:

$$T_{Bsoil,p} = T_{eff} \cdot e_{r,p} \tag{13}$$

CMEM comprises four modules for the computation of the contributions from soil, vegetation, snow and the atmosphere, respectively. The code is designed to be highly modular and for each microwave modelling component, a choice of several parameterisations are considered. Table 2 summarises the modular structure of CMEM and lists for each module the choice of modelling options considered. The brightness temperature at

Module	Variable	Parameterisations		
Soil	ε	Dobson et al. (1985)	Wang and Schmugge (1980)	Mironov et al. (2004)
	T_{eff}	T_{surf} Holmes et al. (2006)	Choudhury et al. (1982)	Wigneron et al. (2001)
	$e_{s,p}$	Fresnel law	Wilheit (1978)	
	$e_{r,p}$	Choudhury et al. (1979(@) Wigneron et al. (2007)	Wigneron et al. (2001) Wegmüller and Mätzler (1999)	SMOS ATBD (2007)
Vegetation	$\tau_{veg,p}$	Wegmüller et al. (1995) Kirdyashev et al. (1979)	Wigneron et al. (2007)	Jackson and O'Neill (1990)
Snow	rsn_p	Pulliainen et al. (1999)		
Atmosphere	$\tau_{atm,p}$	Pellarin et al. (2002)	Liebe (2004)	Ulaby et al. (1986)

Table 2: Modular configuration of CMEM. For each component, the key variable is indicated and the list of options is provided. The soil module includes 4 components: the dielectric mixing model (ε), the effective temperature model (T_{eff}), the smooth surface emissivity model ($e_{s,p}$), the rough surface emissivity, $e_{r,p}$. For each of them several parameterisations are proposed. The vegetation module key variable is the vegetation optical thickness $\tau_{veg,p}$. The snow module computes the snow reflectivity rsn_p and the atmospheric module provides the atmosphere optical thickness $\tau_{atm,p}$.

the top of the vegetation ($T_{Btov,p}$, Equation 12) can be computed for each model grid box taking the sub-grid scale variability of the land surface into account. Up to seven tiles can be considered in each CMEM grid box: bare soil, low vegetation, high vegetation (each are either free of snow or snow-covered) and open water. For low and high vegetation tiles, the dominant type is determined from the land-cover data base. For each grid cell, brightness temperatures are computed separately for each tile. The grid-cell averaged brightness temperature is computed using the weighted sum of each tile.

Several studies have been conducted at ECMWF with CMEM to simulate, calibrate and evaluate the computed brightness temperature at different spatial and temporal scales. Different observing configuration (L-band, C-band, X-band) at several incidence angles have been considered and evaluated as well as different forward modelling approaches. Some of these results are presented hereafter. They provide quantitative assessment of the observation minus model departures and help identify the optimal forward-model configuration prior to the SMOS launch.

5.2 CMEM calibration using Skylab observations

The NASA Skylab mission in 1973-1974 was the first to provide L-band (1.4 GHz) satellite measurements from its S-194 instruments. It performed nadir measurements at a ground resolution of about 110 km (Eagleman and Lin, 1976). Although the observation data set is limited to nine overpasses between June 1973 and January 1974 it is currently the only existing space-borne L-band data set available (Jackson et al., 2004). Moreover, the observations cover a wide range of climates and a variety of biomes.
A calibration study has been conducted by comparing ERA-40 (ECMWF's 40-year climate re-analysis, Uppala and co authors, 2005) based L-band brightness temperatures with the Skylab observations at L-band (Drusch et al., 2008). CMEM input data comprise surface fields from ERA-40, vegetation data from the ECOCLIMAP data set (Masson et al., 2003), and the Food and Agriculture Organization (FAO) soil data base (FAO, 2003). Figure 14 indicates the SKYLAB overpasses and observation dates.

In a first step, different parameterisations for surface roughness and the vegetation optical depth were used to provide an estimate on the corresponding brightness temperature sensitivities. Then the radiometric surface roughness, which has to be estimated and does not feed back to the NWP model, was adjusted to provide

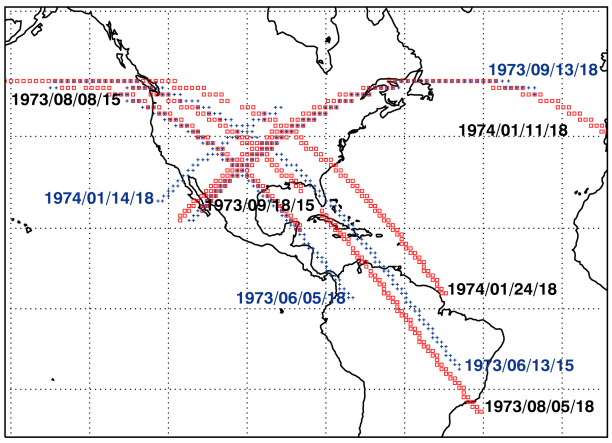

Figure 14: SKYLAB observations at L-band and corresponding data and time (UTC). Blue symbols indicate overpasses for which the data were used for the calibration of CMEM. Validation was performed for data acquired on overpasses indicated in red.

bias free estimates. In total, ten combinations of different roughness and vegetation parameterisations were used to compute brightness temperatures. For these computations the recommended parameter values from the reviewed literature have been adopted. They are performed to gauge the range output values and determine sensitivities. Figure 15a,b shows our reference configuration using parameterisations that have often been applied in the literature.
A second configuration gave promising results when data from field experiments were used (Wigneron et al., 2007). However, in combination with the ECMWF model fields and the NWP auxiliary data sets the systematic and random errors were comparably large. For North America we obtain a correlation coefficient of 0.04 and a bias of 23.1 K (Figure 15c). The corresponding values for the South American data are 0.58 and 27.9 K (Figure 15d). The best results for both continents have been obtained using Wigneron et al. (2001) to describe the effects of surface roughness and Kirdyashev et al. (1979) for the parameterisation of vegetation (Figure 15e,f).

The main results from the calibration study (Drusch et al., 2008) are:

- Calibrating CMEM results in low biases, which are acceptable for data assimilation applications.
- The rather large RMS errors over North America are caused by errors in the ERA-40 soil moisture fields.
- Systematic differences in the dynamic range of the modelled and observed brightness temperatures are an artefact of the NWP model parameters, which define TESSEL's soil moisture climatology.
- These differences can not be reduced in the calibration process but should be corrected through a statistical correction method.

5.3 The SMOSREX field experiment

The SMOSREX (Soil Monitoring Of the Soil Reservoir EXperiment) field experiment site is located near Toulouse, France. For this location a continuous data set from 2003 to 2008 is available comprising in-situ measurements of soil moisture, soil temperature, meteorological variables and multi-angular highly accurate L-band observations (de Rosnay et al., 2006).

Sensitivity studies have been conducted for different incidence angles and different CMEM configurations using (i) the observed data and (ii) output from ECMWF's operational NWP model. In both cases modelled brightness

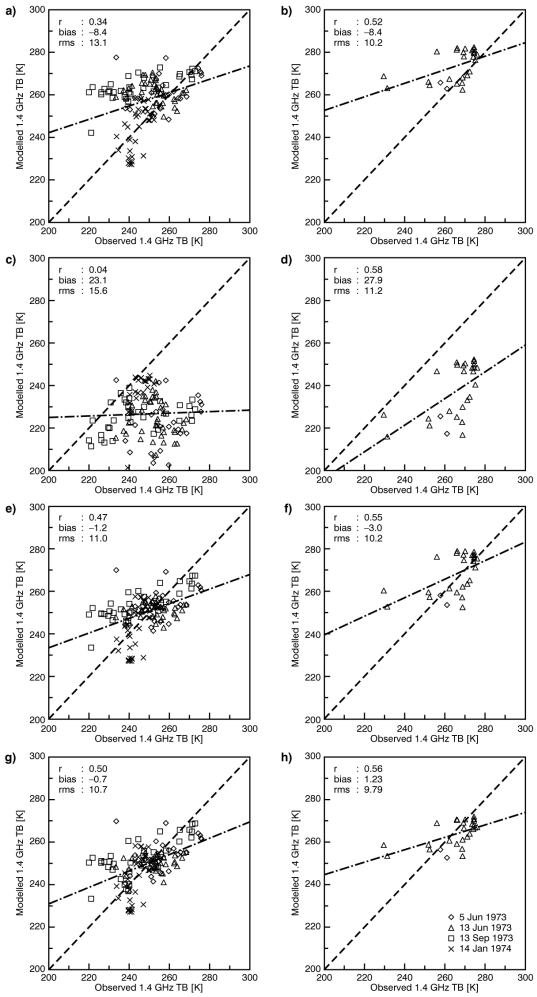

Figure 15: Calibration of the ERA-40 based CMEM simulation at L-band for the SKYLAB overpasses over North America (left) and South America (right). The top panel (a,b) considers the Wigneron et al. (2001) and Jackson and Schmugge (1991) parameterisations for the soil roughness and vegetation optical thickness respectively. The results of the second panel (c,d) are obtained using the parameterisations of Wigneron et al. (2007) for both. Third and fourth panels (e,f,g,h) results are for the Wigneron et al. (2001) soil roughness and the Kirdyashev et al. (1979) vegetation optical thickness, considering different values of the parameters. The dashed-dotted line is the linear regression.

temperatures have been compared against the L-band observations. Here we focus on results obtained using the ECMWF model (with HTESSEL) at T799 spectral resolution. The comparison is based on data for 2004 and we use four statistical indices to assess the quality of the simulations: bias, root mean square error (RMSE), relative explained variance (R^2), and the Nash coefficient.

Figure 16 summarises the comparison between modelled and observed brightness temperatures at vertical polarisation. The statistical indices obtained for two different model configurations are presented as a function of incidence angle. For Wigneron's parameterisation of vegetation optical depth the lowest bias is obtained for an incidence angle of 40 °. The R^2 values indicate that the temporal dynamics are well captured by the ECMWF synthetic brightness temperatures at any incidence angle, although best correlation ($R^2 = 0.82$) is obtained at 50 °. RMSE in simulated brightness temperature increases with the incidence angle and the Nash coefficient suggests the best result for an observing angle of 30 °.

When the Kirdyashev model is used in the forward operator better performances are obtained for incidence

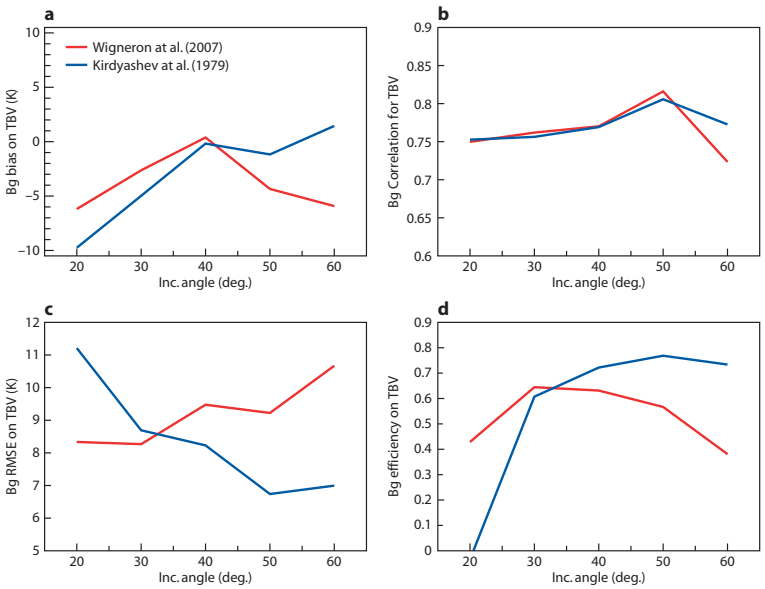

Figure 16: Background error of the ECMWF synthetic brightness temperature (K) over the SMOSREX pixel, as a function of the incidence angle, at vertical polarisation for two different microwave modelling approaches of the vegetation optical depth by Wigneron et al. (2007) and Kirdyashev et al. (1979) (see in Table 2). The top panel shows the bias (left) and the correlation coefficient R^2 (right). The bottom panel shows the RMSE (left) and the Nash coefficient (right).

angles of 40 to 60 ° than for lower angles. Overall, the best modelling/observing configuration is obtained when the Kirdyashev opacity model is used for an observing angle of 50 °. The results also suggest that a future bias correction scheme for SMOS should depend on the viewing angle. The good agreement with R^2 values exceeding 0.7 at vertical polarisation is particularly encouraging, since it applies to both parameterisations and all angles used. We have thus shown that the coupled IFS / CMEM system can capture the main variability on the point scale.

5.4 The ALMIP inter-comparison of microwave emission models

A large-scale CMEM evaluation study for low frequency passive microwave has been conducted at C-band, using the AMSR-E data over West Africa. This work has been conducted with an ensemble of Land Surface Models (LSMs) in the joint framework of the SMOS and the ALMIP (AMMA Land Surface Model Intercomparison Project) projects (Boone and de Rosnay, 2007b). ALMIP is a coordinated land surface modelling activity conducted within the AMMA project. One of its objectives is to address the contribution of soil moisture dynamics to the African monsoon dynamics and variability (Redelsperger et al., 2006).

The Advanced Microwave Scanning Radiometer on Earth Observing System (AMSR-E) on the NASA's AQUA satellite was launched in 2002 and it is still operating. AMSR-E measures microwave brightness temperatures at five frequencies, including C-band and X-band channels (6.9 and 10.7 GHz), with a ground resolution of about 60 km at C-band for an incidence angle of 55 ° (Njoku et al., 2003). AMSR-E products include brightness temperature as well as soil moisture and vegetation water content products. They are archived and distributed routinely by the NASA National Snow and Ice Data Center's (NSIDC) Distributed Active Archive Center (DAAC) (Njoku, 2004).

In the recently completed phase-1 of ALMIP, an ensemble of state-of-the-art LSMs have been run offline (i.e. decoupled from an atmospheric model) at a regional scale over West Africa for five annual cycles (2002 to

2006). Eleven LSMs participated in the inter-comparison (Boone and de Rosnay, 2007b). For ALMIP-MEM (de Rosnay et al., 2008) the eight LSMs that are used for NWP applications were coupled with CMEM (Table 3). All participating LSMs require the following input forcing fields: precipitation, short-wave and long-wave radiative fluxes, wind speed and direction, 2m air humidity and temperature and surface pressure.

For each LSM, two ALMIP experiments were conducted with different precipitation and radiative-flux forcing. In the control experiment (EXP1), the LSMs were forced with the ECMWF forecasts for 2002-2006. In the second experiment (EXP2), ECMWF fields are hybridised with the satellite based precipitation products obtained in EPSAT-SG (Estimation des Pluies par SATellite - Seconde Génération, Chopin et al. (2004)) and the OSI-SAF (Ocean and Sea-Ice - Satellite Application Facility) radiative fluxes. Boone and de Rosnay (2007a) have shown that the hybridised forcing data set used in EXP2 is more realistic. In particular, the extension of the African monsoon to the north is better represented than in the ECMWF model precipitation which underestimates rainfall occurrence and intensity over the Sahel.

Name	Group	Reference
ISBA-FR	CNRM/Météo-France	Noilhan and Planton (1989)
ISBA-DF	CNRM/Météo-France	Boone et al. (2000)
HTESSEL	ECMWF	Balsamo et al. (2008)
TESSEL	ECMWF	Viterbo and Beljaars (1995)
CTESSEL	ECMWF	Jarlan et al. (2007)
JULES	MetOffice	Blyth et al. (2006)
NOAH	NCEP/EMC	Chen and Dudhia (2001)
ORCHIDEE-CWRR	IPSL	de Rosnay et al. (2002)

Table 3: Land Surface Models used for ALMIP-MEM.

Both EXP1 and EXP2 were performed at a 0.5 ° resolution over the West African domain (from 5 °S to 20 °N and from 20 °W to 30 °E). ALMIP outputs have been provided for each ALMIP LSM at a 3 hour time step. They include soil moisture and soil temperature profiles, runoff, sensible and latent heat fluxes. Table 4 summarises the different microwave modelling options tested in ALMIP-MEM.

Figure 17 shows the spatial distributions of observed (AMSR-E) and simulated (ORCHIDEE / CMEM) brightness temperatures at horizontal polarisation on days 200-201 of 2006. The data represent the descending orbit and are based on the configuration using the Mironov model to simulate the dielectric constant and the Kirdyashev parameterisation for the vegetation optical thickness. High values of soil moisture result in low emissions and thus in low brightness temperatures. In contrast, areas with high vegetation water content, as encountered at latitude between 4 °S and 10 °N, have high brightness temperature values. This figure clearly shows the presence of a wet patch centred on 2 °W, 15 °N in the Sahel region. This typically corresponds to the occurrence of a monsoon season meso-scale convective rainfall event. This wet patch is well captured by the EXP2

	Dielectric constant		
Vegetation optical depth	Dobson et al. (1985)	Mironov et al. (2004)	Wang and Schmugge (1980)
Jackson and O'Neill (1990)	1	5	9
Kirdyashev et al.(1979)	2	6	10
Wegmüller et al., (1995)	3	7	11
Wigneron et al. (2007)	4	8	12

Table 4: Physical parameterizations used in CMEM for ALMIP-MEM. Twelve configurations are considered for different combination of soil dielectric and vegetation optical depth models.

ALMIP-MEM simulation. However, it is not captured in EXP1 for which the ECMWF precipitation forcing data have been used. It is clear from this figure that the errors in simulated brightness temperatures will be highly dependent on forecast errors in precipitation. In turn, these results suggest that low-frequency passive microwave observations can detect errors introduced through uncertainties in the precipitation forcing. Figure

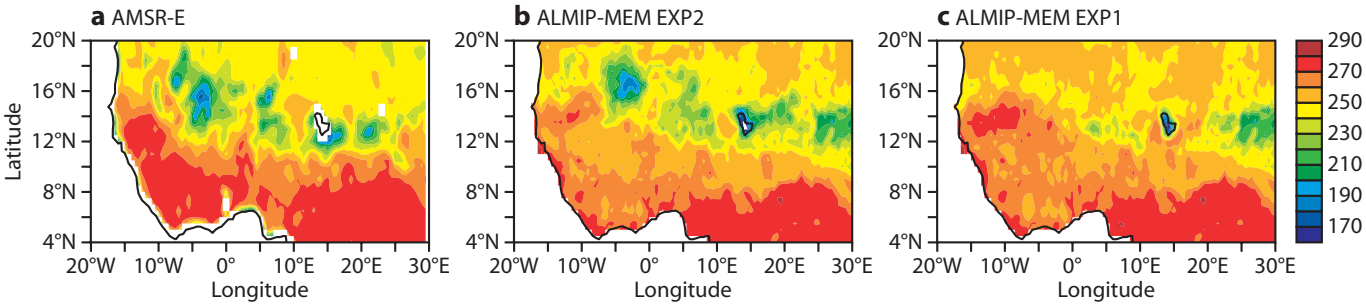

Figure 17: C-band brightness temperature at horizontal polarisation on DoY 200-201: observed by AMSR-E (left), ORCHIDEE simulations in ALMIP-MEM for EXP2 (middle) and EXP1 (right).

18 represents the time-latitude diagram of the horizontally polarised brightness temperatures at C-band from AMSR-E and using the ALMIP-MEM EXP2 and the eight LSMs indicated in Table 3.

For each LSM a bias correction has been applied which subtracts the annual-mean value. The time-latitude diagram (Figure 18) shows the simulated brightness temperature evolutions when CMEM is used with the Kirdyashev vegetation opacity model and the Wand and Schmugge dielectric model. The Kirdyashev vegetation opacity model is the best modelling configuration for any of the considered LSMs. AMSR-E C-band data show a wet patch over Sahel during the rainy season, centred at day 210 and latitude 15.5 ° North. This wet patch is captured by all the LSMs, but the amplitude is either overestimated or underestimated depending on the LSM. However, this figure underlines the general good agreement between the model-based simulations and the satellite data.

Taylor diagrams display the normalised Standard Deviation (SDV) as a radial distance and the correlation between modelled and observed brightness temperatures as an angle in a polar plot. In Figure 19 a) results for the eight LSMs using the same meteorological forcing and one identical CMEM configuration are presented. Figure 19 b) addresses the performances of one LSM (HTESSEL) coupled to different microwave model configurations.

The normalised standard deviations in simulated brightness temperatures for the year 2006 lie in the range of 0.67 to 1.36, and correlation values between modelled and observed brightness temperatures vary between 0.54 and 0.73 (Figure 19 (a)). The scatter for the different LSMs results from differences in land-surface process parameterisations leading to different simulations of soil moisture and soil temperature profiles. In contrast, in Figure 19 (b) one LSM (HTESSEL) is used for several microwave-emission model configurations. The scatter in model performance varies from 1.0 to 1.4 for the SDV and from -0.01 to 0.54 for the correlation. In these simulations, soil moisture and soil temperature profiles are identical, but the parameterisation of the soil dielectric constant and vegetation opacity are different.

The results presented in Figures 19 (a) and (b) clearly show that, in terms of correlation, the scatter due to the microwave emission model is larger than that due to the LSMs. This figure also points out that the Kirdyashev model (numbers 2, 6, 10 in Figure 19 (b) for the Dobson, Mironov and Wang & Schmugge dielectric models respectively) leads to much better performances than the other vegetation opacity models in terms of both SDV and correlation. The scatter due to the soil dielectric constant model is less important than that due to vegetation opacity. Furthermore, it shows that the Wang and Schmugge model provides best results whatever

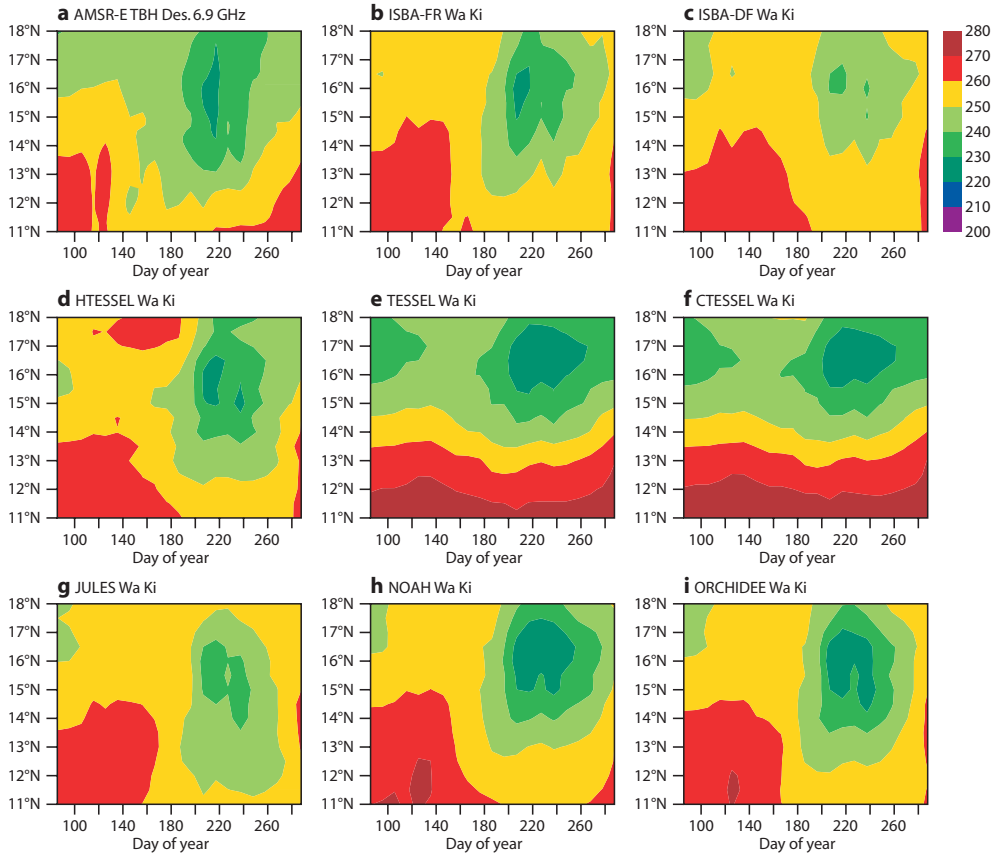

Figure 18: Time-latitude diagram of the horizontally polarised brightness temperature observed by AMSR-E and simulated by ALMIP-MEM for EXP2 (2006). For each ALMIP-MEM simulation a bias correction was applied, specifically computed for each LSM when comparing simulated and observed brightness temperature.

opacity model is used for the vegetation. Results illustrated here with HTESSEL are confirmed for all the ALMIP-MEM LSMs. There is only one LSM (ORCHIDEE) for which the Mironov dielectric model performs slightly better than the Wang and Schmugge model. The robustness of the Kirdyashev vegetation opacity-model to provide best agreement of simulated brightness temperature for different precipitation forcing and different LSMs is particularly noteworthy.

5.5 Passive Microwave summary

L-band brightness temperatures measured by SMOS are a new observation type which has never been used in NWP applications before. Since there are hardly any demonstration data-sets available, the preparation to use the SMOS data is a difficult task. The results summarised in this section are based on different observation systems deployed at different times and locations capturing processes at various scales. However, the findings are consistent in that the importance of the forward operator, i.e. the microwave emission model, has been evidenced. In addition, the key parameterisations have been identified and we have shown that the resulting brightness temperatures resemble the main signatures obtained from the corresponding observations. Implementation of CMEM in the IFS will ensure monitoring of SMOS observations from shortly after its launch in 2009.

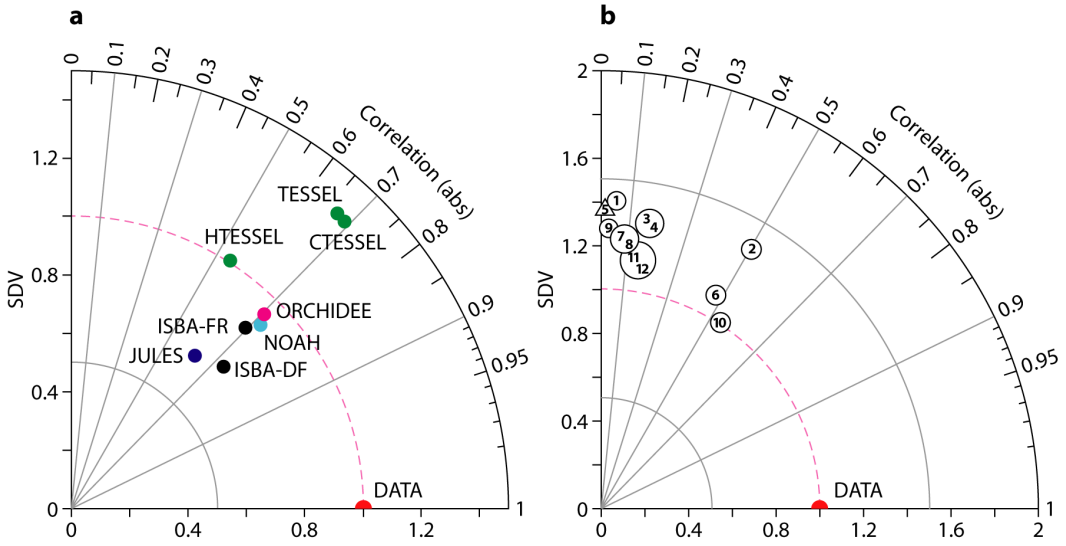

Figure 19: Taylor diagram illustrating the statistics of the comparison between ALMIP-MEM synthetic brightness temperature and AMSR-E data at C-band for (a) different LSMs coupled to CMEM using the Wang and Schmugge dielectric model coupled to the Kirdyashev vegetation opacity model, (b) the HTESSEL LSM coupled to CMEM using different configurations of the microwave emission modelling. The numbers indicated within the circle (right) refer to the vegetation opacity and dielectric models combination obtained from Table 4. Note that the radial axis scale is different for (b).

6 Summary and outlook

ECMWF's current operational land surface analysis system is based on an optimum interpolation scheme of 2 m temperature (T_{2m}) and 2 m relative humidity (RH_{2m}). For soil moisture it is shown that this scheme efficiently improves the turbulent surface fluxes and the weather forecast on large geographic domains while root zone soil moisture acts as a "sink" variable, in which errors are allowed to accumulate. Satellite observations provide more direct estimates of surface soil moisture conditions which can complement the classical soil moisture analysis.

In order to take full advantage of all available data, an EKF surface analysis system has been developed at ECMWF and implemented in the IFS. It enables combined assimilation of observations of various kinds (screen level parameters and active and passive microwave); it considers the observation and model errors during the analysis in a statistically optimal way and allows assimilation of the observation at the correct observation time. However, combining the different data sets in the EKF surface analysis is a major challenge considering that the temporal and spatial structure of model and observation errors need to be specified accurately. The recently revised land surface model HTESSEL is an important component of the EKF surface analysis. Accounting for soil texture and infiltration properties in HTESSEL allows to simulate soil moisture dynamics in the correct range and with the correct dynamics. This ensures consistency between background variables (soil moisture), forward and observed variables (e.g. soil moisture index, brightness temperature).

First results using the EKF surface analysis are presented in this paper. When the screen level parameters are assimilated, the EKF gain coefficients and soil moisture increments present patterns similar to those obtained with the OI surface analysis. But their values are generally lower for the EKF than for the OI. In contrast to the OI, the EKF surface analysis enables different amplitudes of the increments for the different soil layers, in agreement with physical processes governing the vertical diffusion of soil temperature and soil moisture.

In parallel to the EKF development and implementation, our investigation has been focused in the past two

years on the development and validation of observation operators for both active and passive microwave soil moisture and brightness temperature data. The observation operators are of highest importance to account for satellite data in the EKF soil moisture analysis. Active microwave scatterometer observations (such as ERS and ASCAT) contain valuable information about surface soil moisture which our results confirm. Our comparisons against nine years of ERA-40 re-analysis indicates a correlation of up to 0.7 for anomalies over large parts of the land surface. The observation operator used to transform the non-dimensional soil moisture index to the model equivalent soil moisture has been developed. It is based on cumulative distribution function (CDF) matching. ASCAT soil moisture data are assimilated in the EKF surface analysis system for a 1-month experiment, showing that soil moisture increments mainly concern the uppermost soil layer.

Passive microwave remote sensing is also a very promising approach for the global monitoring of surface soil moisture. C-band AMSR-E and L-band SMOS brightness temperatures data will be monitored and assimilated in ECMWF's global NWP system to quantify the impact of this new observation type on the forecast quality. To this end the Community Microwave Emission Model (CMEM) has been developed at ECMWF as the forward operator for low-frequency passive microwave brightness temperatures at 1 to 20 GHz. CMEM has been calibrated and validated based on different observation systems (Skylab, SMOSREX, AMSR-E) deployed at different times and locations capturing processes at various scales. Key parameterisations have been identified and we have shown that the resulting brightness temperatures resemble the main signatures obtained from the corresponding observations. By implementing CMEM in the IFS we will enable monitoring of SMOS observations from shortly after its launch from 2009 onwards.

So far, no satellite data have been used in the operational surface analysis, whereas more than 16 million observations per day are used for the atmospheric analysis. It is somewhat surprising that the forecasts quality is good although the surface parameter are not particularly accurate. This is explained by the fact that the current operational surface analysis and the land surface model are tuned to provide correct fluxes and lower atmospheric parameters rather than accurate surface variables. The skill of the forecasts is mainly evaluated using variables describing the large scale dynamics, e.g. geopotential height of 500 hPa. But new applications (e.g. carbon cycle and crop modelling, water resources management) rely on accurate hydrological parameters and surface variables. Furthermore there is now an increasing emphasis on verification in terms of near surface weather parameters (e.g. ground precipitation or 2m temperatures). The ECMWF EKF surface analysis system, which allows to include various satellite measurements, has been developed in the framework.

The EKF surface analysis is currently under evaluation in the research branch and it is expected to be used operationally by the end of 2009. In addition, a stand-alone version of the EKF surface analysis will be developed in 2009. This will enable a more modular assimilation scheme which will be portable and accessible for the land surface modelling and remote sensing communities. The stand-alone EKF surface analysis will provide a valuable tool for further developments, evaluation and validation of multi-sensor assimilation of land surface data. A comprehensive verification strategy will be developed. Since the land surface is very inhomogeneous this should comprise in-situ observations, area averages from regional networks and large scale approaches using integrated parameters such as modelled atmospheric moisture convergence estimates and river run-off measurements.

This study focuses on the soil moisture analysis with screen level and satellite data from ASCAT and (future) SMOS observations. The EKF surface analysis also opens future possibilities to analyse other variables, e.g. snow depth and fractional coverage, and vegetation parameters.

Acknowledgements

The authors thank Anton Beljaars and Jean-François Mahfouf for their comments on the paper and on the EKF surface analysis results. Work on active and passive microwave soil moisture remote sensing was funded by the EUMETSAT H-SAF project and the ESA's SMOS project.

References

Balsamo, G., F. Bouyssel, and J. Noilhan, 2004: A simplified bi-dimensional variational analysis of soil moisture from screen-level observations in a mesoscale numerical weather prediction model. *Q. J. R. Meteorol. Soc.*, , 895–915.

Balsamo, G., J.-F. Mahfouf, S. Bélair, and G. Deblonde, 2007: A land data assimilation system for soil moisture and temperature: An information content study. *J. Hydromet.*, **8**, 1225–1242.

Balsamo, G., P. Viterbo, A. Beljaars, B. van den Hurk, M. Hirsch, A. Betts, and K. Scipal, 2008: A revised hydrology for the ECMWF model: Verification from field site to terrestrial water storage and impact in the Integrated Forecast System. *ECMWF Tech. Memo. 563; also submitted to Journal of Hydrometeorology*, .

Bartalis, Z., W. Wagner, V. Naeimi, S. Hasenauer, K. Scipal, H. Bonekamp, J. Figa, and C. Anderson, 2007: Initial soil moisture retrievals from the metop-a advanced scatterometer (ASCAT). *Geophys. Res. Let.*, **34**, doi:10.1029/2007GL031088.

Bélair, S., L.-P. Crevier, J. Mailhot, B. Bilodeau, and Y. Delage, 2003: Operational implementation of the ISBA land surface scheme in the Canadian regional weather forecast model. Part I: Warm season results. *J. Hydromet.*, **4**, 352–470.

Betts, A. K., J. H. Ball, A. G. Barr, T. A. Black, J. H. McCaughey, and P. Viterbo, 2006: Assessing land-surface-atmosphere coupling in the era-40 reanalysis with boreal forest data. *Agric. For. Meteorol.*, **140**, 365–382.

Blyth, E., M. Best, P. Cox, R. Essery, O. Boucher, R. Harding, C. Prentice, P. Vidale, and I. Woodward, 2006: JULES: a new community land surface model. *IGBP Newsletter, October*, .

Boone, A., and P. de Rosnay, 2007a: AMMA forcing data for a better understanding of the West African monsoon surface-atmosphere interactions. Quantification and Reduction of Predictive Uncertainty for Sustainable Water Resource Management. *IAHS Publ.*, **303**.

Boone, A., and P. de Rosnay, 2007b: Toward the improved understanding of land-surface processes and coupling with the atmosphere over West Africa. *LEAPS Newsletter 3*, .

Boone, A., V. Masson, T. Meyers, and J. Noilhan, 2000: The Influence of the Inclusion of Soil Freezing on Simulations by a SoilVegetationAtmosphere Transfer Scheme. *J. Appl. Meteorol.*, **39(9)**.

Bouttier, F., J.-F. Mahfouf, and J. Noilhan, 1993: Sequential assimilation of soil moisture from atmospheric low-level parameters. Part I: Sensitivity and calibration studies. *J. Appl. Met.*, **32**, 1335–1351.

Calvet, J.-C., J. Noilhan, and P. Bessemoulin, 1998: Retriving the root-zone soil moisture from surface soil moisture or temperature estimates : a feasibility study based on field measurements. *J. Appl. Meteorol.*, **37**, 371–386.

Ceballos, A., K. Scipal, W. Wagner, and J. Martinez-Fernandez, 2005: Validation and downscaling of ers scatterometer derived soil moisture data over the central part of the duero basin, spain. *Hydrol. Proc.*, **19**, 1549–1566.

Chen, F., and J. Dudhia, 2001: Coupling an advanced land surface-hydrology model with the Pen State-NCAR MM5 modeling system. Part I: Model implementation and sensitivity. *Mon. Wea. Rev*, **129**.

Chopin, F., J. Berges, M. Desbois, I. Jobard, and T. Lebel, 2004: Multi-scale precipitation retrieval and validation in african monsoon systems. *2nd International TRMM Science Conf., 6-10 Spet. Nara, Japan*, .

Choudhury, B., T. Schmugge, A. Chang, and R. Newton, 1979: Effect of surface roughness on the microwave emission from soils. *J. Geophys. Res.*, , 5699–5706.

Choudhury, B., T. Schmugge, and T. Mo, 1982: A parameterization of effective soil temperature for microwave emission. *J. Geophys. Res.*, , 1301–1304.

Clapp, R. B., and G. M. Hornberger, 1978: Empirical equations for some soil hydraulic properties. *Water Resources Res.*, **14**, 601–604.

Cosby, B. J., G. M. Hornberger, R. B. Clapp, and T. Ginn, 1984: A statistical exploration of the relationships of soil moisture characteristics to the physical properties of soils. *Water Resources Res.*, **20**, 682–690.

Crow, W., and E. Wood, 2003: The assimilation of remotely sensed soil brightness temperature imagery into a land surface model using ensemble filtering: A case study based on ESTAR measurements during SGP97. *Adv. Water Res.*, **26**, 137–149.

Crow, W., and X. Zhan, 2007: Continental-scale evaluation of remotely sensed soil moisture products. *IEEE Geosc. Rem. Sens. Let.*, **4**, 451–455.

de Rosnay, P., J.-C. Calvet, Y. H. Kerr, J.-P. Wigneron, F. Lemaître, M.-J. Escorihuela, J. Muñoz Sabater, K. Saleh, J. Barrié, G. Bouhours, L. Coret, G. Cherel, G. Dedieu, R. Durbe, N. Fritz, F. Froissard, J. Hoedjes, A. Kruszewski, F. Lavenu, D. Suquia, and P. Waldteufel, 2006: SMOSREX: A long term field campaign experiment for soil moisture and land surface processes remote sensing. *Remote sensing of Env.*, **102**, pp 377–389; doi:10.1016/j.rse.2006.02.021.

de Rosnay, P., J. Polcher, M. Bruen, and K. Laval, 2002: Impact of a physically based soil water flow and soil-plant interaction representation for modeling large scale land surface processes. *J. Geophys. Res.*, **107**.

de Rosnay, P., M. Drusch, A. Boone, G. Balsamo, B. Decharme, P. Harris, Y. Kerr, T. Pellarin, J. Polcher, and J.-P. Wigneron, 2008: Microwave land surface modelling evaluation against amsr-e data over west africa. the amma land surface model intercomparison experiment coupled to the community microwave emission model (almip-mem). *ECMWF Tech. Memo 565; also submitted to J. Geophys. Res*, .

de Wit, A., and C. van Diepen, 2007: Crop model data assimilation with the ensemble kalman filter for improving regional crop yield forecasts. *Agr. Forest Met.*, **146**, 38–56.

Deardorff, J. W., 1978: Efficient prediction of ground surface temperature and moisture, with inclusion of a layer of vegetation. *J. Geophys. Res.*, **83C**, 1889–1903.

Dickinson, R., A. Henderson-Sellers, and P. Kennedy, 1993: Biosphere-atmosphere transfer scheme (BATS) version 1e as coupled to the NCAR community climate model. *Technical Report NCAR/TN-387 + STR*, . NCAR Boulder, Colorado.

Dirmeyer, P., Z. Guo, and X. Gao, 2004: Comparison, validation, and transferability of eight multiyear global soil wetness products. *J. Hydromet.*, **5(6)**, DOI: 10.1175/JHM-388.1 1011–1033.

Dobson, M., F. Ulaby, M. Hallikainen, and M. El-Rayes, 1985: Microwave dielectric behavior of wet soil-partii: Dielectric mixing models. *IEEE Trans Geosc. Sci*, **38**, 1635–1643.

Douville, H., P. Viterbo, J.-F. Mahfouf, and A. Beljaars, 2000: Evaluation of the Optimum Interpolation and Nudging technique for soil moisture analysis using FIFE data. *Mon. Wea. Rev.*, **128**, 1733–1756.

Drusch, M., 2005: Snow analyses. *Proceedings of the ECMWF / ELDAS workshop on Land Data Assimilation*, **ECMWF, UK**, 105–114.

Drusch, M., 2007: Initializing numerical weather prediction models with satellite-derived surface soil moisture: Data assimilation experiments with ECMWF's Integrated Forecast System and the TMI soil moisture data set. *J. Geophys. Res.*, **112**, doi:10.1029/2006JD007478.

Drusch, M., T. Holmes, P. de Rosnay, and G. Balsamo, 2008: Comparing ERA-40 based L-band brightness temperatures with Skylab observations: A calibration / validation study using the Community Microwave Emission Model. *ECMWF Tech. Memo 566; and J. Hydrometeo. DOI: 10.1175/2008JHM964.1*, .

Drusch, M., D. Vasilievic, and P. Viterbo, 2004: ECMWF's global snow analysis: Assessment and revision based on satellite observations. *J. Appl. Met.*, **43**, 1282–1294.

Drusch, M., and P. Viterbo, 2007: Assimilation of screen-level variables in ECMWF's Integrated Forecast System: A study on the impact on the forecast Quality and analyzed soil moisture. *Monthly Weather Review*, **135**, 300–314.

Drusch, M., E. Wood, and H. Gao, 2005: Observation operators for the direct assimilation of TRMM Microwave Imager retrieved soil moisture. *Geophys. Res. Let.*, **32**.

Drusch, M., E. Wood, and T. Jackson, 2001: Vegetative and atmospheric corrections for soil moisture retrieval from passive microwave remote sensing data: Results from the Southern Great Plains Hydrology Experiment 1997. *J. Hydromet.*, **2**, 181–192.

Eagleman, J., and W. Lin, 1976: Remote sensing of soil moisture by a 21-cm passive radiometer. *J. Geophys. Res.*, **81**, 3660–3666.

FAO, 2003: Digital soil map of the world (DSMW). Tech. rep. re-issued version.

Ferranti, L., and P. Viterbo, 2006: The European summer of 2003: Sensitivity to soil water initial conditions. *J. Climate*, **19(15)** 3659–3680 DOI: 10.1175/JCLI3810.1.

Gedney, N., P. Cox, H. Douville, J. Polcher, and P. Valdes, 2000: Characterizing GCM land surface schemes to understand their responses to climate change. *J. Climate*, **13**, 3066–3079.

Giard, D., and E. Bazile, 2000: Implementation of a new assimilation scheme for soil and surface variables in a global NWP model. *Mon. Wea. Rev.*, **128**, 997–1015.

Grumbine, R., 1996: Automated passive microwave sea ice concentration analysis at NCEP. NOAA NCEP Tech Note 120, 13 pp, [Available online at http://polar.ncep.noaa.gov/seaice/icegroup.html].

Haseler, J., 2004: Early-delivery suite. Technical Memorandum 454, 35 pp, [Available through ECMWF, Reading, UK].

Hess, R., 2001: Assimilation of screen-level observations by variational soil moisture analysis. *Meteorol. Atmos. Phys.*, **77**, 145–154.

Hillel, D. *Environmental soil physics*. Academic Press, San Diego, CA, 1982.

Holmes, T., P. de Rosnay, R. de Jeu, J.-P. Wigneron, Y. Kerr, J.-C. Calvet, M.-J. Escorihuela, K. Saleh, and F. Lemaître, 2006: A new parameterization of the Effective Temperature for L-band Radiometry. *Geophy. Res. Letters*, **33**, L07405, doi:10.1029/2006GL025724.

Jackson, T. J., A. Y. Hsu, A. V. de Griend, and J. R. Eagleman, 2004: Skylab l-band microwave radiometer observations of soil moisture revisited. *International Journal of Remote Sensing*, **25**, 2585–2606.

Jackson, T., and P. O'Neill, 1990: Attenuation of soil microwave emission by corn and soybeans at 1.4and 5 ghz. *IEEE Trans. Geosc. Remote Sens.*, **28(5)**, 978–980.

Jackson, T., and T. Schmugge, 1991: Vegetation effects on the microwave emission of soils. *Remote sens. environ.*, **36**, 203–212.

Jacquemin, B., and J. Noilhan, 1990: Sensitivity study and validation of a land-surface parameterization using the HAPEX-MOBILHY data set. *Boundary-Layer Meteorol.*, **52**, 93–134.

Jarlan, L., G. Balsamo, S. Lafont, A. Beljaars, J.-C. Calvet, and E. Mougin, 2007: Analysis of Leaf Area Index in the ECMWF land surface scheme and impact on latent heat and carbon fluxes: Applications to West Africa. Tech. rep.

Kerr, Y., 2007: Soil Moisture from space: Where we are ? *Hydrogeology journal*, **15**, 117–120.

Kerr, Y., P. Waldteufel, J.-P. Wigneron, J.-M. Martinuzzi, J. Font, and M. Berger, 2001: Soil moisture retrieval from space: The soil moisture and ocean salinity (smos) mission. *IEEE Trans. Geosc. Remote Sens.*, **39 (8)**, 1729–1735.

Kirdyashev, K., A. Chukhlantsev, and A. Shutko, 1979: Microwave radiation of the earths surface in the presence of vegetation cover. *Radiotekhnika i Elektronika*, **24**, 256–264.

Koster, R. et al., 2004: Regions of strong coupling between soil moisture and precipitation. *Science*, **305**, 1138–1140.

Lehner, B., and P. Döll, 2004: Development and validation of a global database of lakes, reservoirs and wetlands. *J. Hydrology*, **296(1-4)**, 1.

Liebe, H., 2004: MPM- An atmospheric millimeter-wave propagation model. *Int. J. Infrared Millimeter Waves*, **10**, 631–650.

Loveland, T. R., B. C. Reed, J. F. Brown, D. O. Ohlen, Z. Zhu, L. Youing, and J. W. Merchant, 2000: Development of a global land cover characteristics database and IGB6 DISCover from the 1km AVHRR data. *Int. J. Remote Sensing*, **21**, 1303–1330.

Mahfouf, J., 1991: Analysis of soil moisture from near-surface parameters. A feasibility study. *J. Appl. Met.*, **7**, 506–526.

Mahfouf, J.-F., K. Bergaoui, C. Draper, F. Bouyseel, F. Taillefer, and L. Taseva, 2008: Comparative study of two offline soil analysis schemes using screen-level observations. *Mon. Weath. Rev.*, , submitted.

Mahfouf, J., P. Viterbo, H. Douville, A. Beljaars, and S. Saarinen, 2000: A Revised land-surface analysis scheme in the Integrated Forecasting System. *ECMWF Newsletter, Summer-Autumn*, .

Mahrt, L., and H.-L. Pan, 1984: A two-layer model of soil hydrology. *Boundary-Layer Meteorol.*, **29**, 1–20.

Masson, V., J.-L. Champeaux, F. Chauvin, C. Meriguet, and R. Lacaze, 2003: A global database of land surface parameters at 1-km resolution in meteorological and climate models. *J. Climate*, **97(1r61)**, 1261–1282.

Mironov, V., M. Dobson, V. Kaupp, S. Komarov, and V. Kleshchenko, 2004: Generalized refractive Mixing dielectric model for moist soils. *Soil Sci. Soc. Am. J.*, **42(4)**, 773–785.

Njoku, E., 2004: updated daily. AMSR-E/AQUA daily L3 surface soil moisture, interpretive parms, & QC EASE-Grids. *Boulder, CO, USA: National Snow and Ice Data Center*, **Digital Media**.

Njoku, E., T. Jackson, V. Lakshmi, T. Chan, and S. Nghiem, 2003: Soil moisture retrieval from AMSR-E. *IEEE Trans. Geosc. Remote Sens.*, **41(2)**, 215–229.

Noilhan, J., and S. Planton, 1989: A simple parameterization of land-surface processes for meteorological models. *Mon. Wea. Rev.*, **117**, 536–549.

Parajka, J., V. Naeimi, G. Blöschl, W. Wagner, R. Merz, and K. Scipal, 2006: Assimilating scatterometer soil moisture data into conceptual hydrologic models at the regional scale. *Hydr. Earth Sys. Sci.*, **10**, 353–368.

Pauwels, V., R. Hoeben, N. Verhoest, F. D. Troch, and P. Troch, 2002: Improvement of TOPLATS-based discharge predictions through assimilation of ERS-based remotely sensed soil moisture values. *Hydrol. Processes*, **16**, 995–1013.

Pauwels, V., and G. D. Lannoy, 2006: Improvement of modeled soil wetness conditions and turbulent fluxes through the assimilation of observed discharge. *J. Hydromet.*, **7**, in press.

Pellarin, T., J.-P. Wigneron, J.-C. Calvet, M. Berger, H. Douville, P. Ferrazzoli, Y. Kerr, E. Lopez-Baeza, J. Pulliainen, L. Simmonds, and P. Waldteufel, 2002: Two-year global simulation of L-band brightness temperature over land. *IEEE Trans. Geosc. Remote Sens.*, **41(4)**, 2135–2139.

Pulliainen, J., M. Hallikainen, and J. Grandell, 1999: HUT snow emission model and its applicability to snow water equivalent retrieval. *IEEE Trans. Geos. Remot. Sens*, **37**, 1378–1390.

Redelsperger, J.-L., C. Thorncroft, A. Diedhiou, T. Lebel, D. Parker, and J. Polcher, 2006: African Monsoon, Multidisciplinary Analysis (AMMA): An International Research Project and Field Campaign. *Bull. Amer. Meteorol. Soc*, **87(12)**, 1739–1746.

Reichle, R., D. Entekhabi, and D. McLaughlin, 2001: Downscaling of radiobrightness measurements for soil moisture estimation: A four-dimensional variational data assimilation approach. *Wat. Res. Res.*, **31**, 2353–2364.

Reichle, R., and R. Koster, 2005: Global assimilation of satellite surface soil moisture retrievals into the NASA catchment land surface model. *Geophys. Res. Let.*, **32**, 2353–2364.

Reichle, R., and R. Koster, 2004: Bias reduction in short records of satellite soil moisture. *Geophys. Res. Let.*, **31**, doi:10.1029/2004GL020938.

Reichle, R., R. Koster, P. Liu, S. Mahanama, E. Njoku, and M. Owe, 2007: Comparison and assimilation of global soil moisture retrievals from the advanced microwave scanning radiometer for the earth observing system (amsr-e) and the scanning multichannel microwave radiometer (smmr). *J. Geophys. Res.*, **112**, doi:10.1029/2006JD008033.

Richards, L. A., 1931: Capillary conduction of liquids through porous mediums. *Physics*, **1**, 318–333.

Rodriguez, A., B. Navascues, J. Ayuso, and S. Järvenoja, 2003: Analysis of surface variables and parameterization of surface processes in HIRLAM. Part I: Approach and verification by parallel runs. *HIRLAM technical report No 59, Norrköping, Sweden*, , 52pp.

Rutherford, I., 1972: Data assimilation by statistical interpolation of forecast error fields. *J. Atmos. Sci.*, **29**, 809–815.

Saunders, R., M. Matricardi, and P. Brunel, 1999: An improved fast radiative transfer model for assimilation of satellite radiance observations. *Quart. J. Roy. Met. Soc.*, **125**, 1407–1425.

Schär, C., D. Luethi, U. Beyerle, and E. Heise, 1999: The soil - precipitation feedback: A process study with a regional climate model. *J. Climate*, **12**, 722–741.

Scipal, K., 2002: Global soil moisture monitoring using ers scatterometer data. Phd, Vienna University of Technology.

Scipal, K., C. Scheffler, and W. Wagner, 2005: Soil moisture-runoff relation at the catchment scale as observed with coarse resolution microwave remote sensing. *Hydr. Earth Sys. Sci.*, **9**, 173–183.

Scipal, K., M. Drusch, and W. Wagner, 2008: Assimilation of a ERS scatterometer derived soil moisture index in the ecmwf numerical weather prediction system. *Advances in water resources*, **doi:10.1016/j.advwatres.2008.04013**.

Seuffert, G., P. Gross, C. Simmer, and E. Wood, 2002: The influence of hydrologic modelling on the predicted local weather: Two-way coupling of a mesoscale weather prediction model and a land surface hydrologic model. *J. Hydromet.*, **3**, 505–523.

Seuffert, G., H. Wilker, P. Viterbo, M. Drusch, and J. Mahfouf, 2004: On the usage of screen level parameters and microwave brightness temperature for soil moisture analysis. *J. Hydromet.*, **5**, 516–531.

Shukla, J., and Y. Mintz, 1982: Influence of the land surface evapotranspiration on the Earth's climate. *Science*, **215**, 1498–1501.

SMOS ATBD, 2007: SMOS Expert Support Laboratories, SMOS level 2 Processor for Soil Moisture Algorithm Theoretical Based Document (ATBD). *SO-TN-ESL-SM-GS-0001, issue 2.a*, , 124.

Stark, J., C. Donlon, M. Martin, and M. McCulloch, 2007: Ostia: An operational, high resolution, real time, global sea surface temeprature analysis system. *IEEE OCEANS2007-Europe*, , doi:10.1109/OCEANSE.2007.4302251.

Ulaby, F., R. Moore, and A. Fung. *Microwave remote sensing: active and passive, Vol III, from theory to application*. Artech House, Dedham, MA, 1986.

Uppala, S., and . co authors, 2005: The ERA-40 re-analysis. *Quart. J. Roy. Meteorol. Soc.*, **131**, 2961–3012.

van den Hurk, B., J. Ettema, and P. Viterbo, 2008: Analysis of soil moisture Changes in Europe during a single growing season in a new ECMWF soil moisture assimilation system. *J. Hydromet.*, **9**, 116–131.

Van den Hurk, B. J. J. M., P. Viterbo, A. C. M. Beljaars, and A. K. Betts, 2000: Offline validation of the ERA40 surface scheme. *ECMWF Tech. Memo. No. 295*, .

van den Hurk, B., W. Bastiaanssen, H. Pelgrum, and E. V. Meijgaard, 1997: A new methodology for assimilation of initial soil moisture fields in weather prediction models using Meteosat and NOAA data. *J. Appl. Met.*, **37**, 1217–1233.

van den Hurk, B., L. Graham, and P. Viterbo, 2002: Comparison of land surface hydrology in regional climate simulations of the Baltic Sea catchment. Journal of Hydrology*, **255(1)**, pp. 169-193;* also published in 2001 as ECMWF Technical Memorandum 344.

van den Hurk, B., M. Hirschi, C. Schär, G. Lenderink, E. van Meijgaard, A. van Ulden, B. Rockel, S. Hagemann, L. Graham, E. Kjellstroem, and R. Jones, 2005: Soil control on runoff response to climate change in regional climate model simulations. *J. Climate*, **18**, 3536–3551.

van Storch, H., and W. Zwiers. *Statistical Analysis in Climate Research*. Cambridge University Press, Cambridge, 1999.

Viterbo, P., and A. C. M. Beljaars, 1995: An improved land surface parametrization scheme in the ECMWF model and its validation. *ECMWF Tech. Report No. 75*, . Research Department, ECMWF.

Viterbo, P., A. C. M. Beljaars, J.-F. Mahouf, and J. Teixeira, 1999: The representation of soil moisture freezing and its impact on the stable boundary layer. *Q. J. R. Meteorol. Soc.*, **125**, 2401–2426.

Wagner, W., G. Lemoine, and H. Rott, 1999: A method for estimating soil moisture from ers scatterometer and soil data. *Rem. Sens. Env.*, **70**, 191–207.

Wagner, W., K. Scipal, C. Pathe, D. Gerten, W. Lucht, and B. Rudolf, 2003: Evaluation of the agreement between the first global remotely sensed soil moisture data with model and precipitation data. *J. Geoph. Res.*, **108**, doi:10.1029/2003JD003663.

Walker, J., G. Willgoose, and J. Kalma, 2002: Three-dimensional soil moisture profile retrieval by assimilation of near-surface measurements: Simplified Kalman filter covariance forecasting and field application. *Wat. Res. Res.*, **38**, doi:10.1029/2002WR001545.

Wallace, J. S., I. R. Wright, J. B. Stewart, and C. J. Holwill, 1991: The sahelian energy balance experiment (SEBEX): ground based measurements and their potential for spatial extrapolation using satellite data. *Adv. Space Res.*, **11**, 31–41.

Wang, J., and T. Schmugge, 1980: An empirical model for the complex dielectric permittivity of soils as a function of water content. *IEEE Trans. Geosc. Remote Sens.*, **18**, 288–295.

Warrilow, D. L., A. B. Sangster, and A. Slingo, 1986: Modelling of land-surface processes and their influence on European climate. *UK Met Office Report, Met O 20, Tech Note 38*, .

Wegmüller, U., and C. Mätzler, 1999: Rough bare soil reflectivity model. *IEEE Transactions on Geoscience Electronics*, **37**, 1391–1395.

Wegmüller, U., C. Mätzler, and E. Njoku, 1995: Canopy opacity models, in passive microwave remote sensing of land-atmosphere interactions. *B. et al. Ed. Utrecht, The Netherlands: VSP*, , 375.

Wigneron, J.-P., Y. Kerr, P. Waldteufel, K. Saleh, M.-J. Escorihuela, P. Richaume, P. Ferrazzoli, P. de Rosnay, R. Gurney, J.-C. Calvet, M. Guglielmetti, B. Hornbuckle, C. Mätzler, T. Pellarin, and M. Schwank, 2007: L-band Microwave Emission of the Biosphere (L-MEB) Model: description and calibration against experimental data sets over crop fields. *Remote sens. environ.*, **107**, 639–655.

Wigneron, J.-P., L. Laguerre, and Y. Kerr, 2001: A Simple Parmeterization of the L-band Microwave Emission from Rough Agricultural Soils. *IEEE Trans. Geosc. Remote Sens.*, **39**, 1697–1707.

Wilheit, T., 1978: Radiative transfert in plane stratified dielectric. *IEEE Transactions on Geoscience Electronics*, **16(2)**, 138–143.

Zhao, D., B. Su, and M. Zhao, 2006: Soil moisture retrieval from satellite images and its application to heavy rainfall simulation in eastern china. *Adv. Atmos. Sc.*, **23(2)**, 299–316.